atoms

MDPI

Article

Transitional Strength Under Plasma: Precise Estimations of Astrophysically Relevant Electromagnetic Transitions of Ar^{7+}, Kr^{7+}, Xe^{7+}, and Rn^{7+} Under Plasma Atmosphere

Swapan Biswas [1], Anal Bhowmik [2,3], Arghya Das [4], Radha Raman Pal [1] and Sonjoy Majumder [4,*]

[1] Department of Physics, Vidyasagar University, Midnapore 721102, India; biswas.swapan25@gmail.com (S.B.); rrpal@mail.vidyasagar.ac.in (R.R.P.)
[2] Department of Physics, University of Haifa, Haifa 3498838, Israel
[3] Haifa Research Center for Theoretical Physics and Astrophysics, University of Haifa, Haifa 3498838, Israel
[4] Department of Physics, Indian Institute of Technology Kharagpur, Kharagpur 721302, India
* Correspondence: sonjoym@phy.iitkgp.ac.in

Highlights:

What are the main findings?

- Atomic spectroscopy for Ar^{7+}, Kr^{7+}, Xe^{7+}, and Rn^{7+} ions with high accuracy.
- Plasma screened ionization potential, atomic transition amplitudes and rates.
- Ionisation potential depression parameters.

What is the implication of the main finding?

- Properties of the astrophysical medium.
- Properties of laboratory plasma.

Abstract: The growing interest in atomic structures of moderately stripped alkali-like ions in the diagnostic study and modeling of astrophysical and laboratory plasma makes an accurate many-body study of atomic properties inevitable. This work presents transition line parameters in the absence or presence of plasma atmosphere for astrophysically important candidates Ar^{7+}, Kr^{7+}, Xe^{7+}, and Rn^{7+}. We employ relativistic coupled-cluster (RCC) theory, a well-known correlation exhaustive method. In the case of a plasma environment, we use the Debye Model. Our calculations agree with experiments available in the literature for ionization potentials, transition strengths of allowed and forbidden selections, and lifetimes of several low-lying states. The unit ratios of length and velocity forms of transition matrix elements are the critical estimation of the accuracy of the transition data presented here, especially for a few presented for the first time in the literature. We do compare our findings with the available recent theoretical results. Our reported data can be helpful to the astronomer in estimating the density of the plasma environment around the astronomical objects or in the discovery of observational spectra corrected by that environment. The present results should be advantageous in the modeling and diagnostics laboratory plasma, whereas the calculated ionization potential depression parameters reveal important characteristics of atomic structure.

Keywords: atomic data; transition probability; oscillator strength; lifetime; plasma density

Citation: Biswas, S.; Bhowmik, A.; Das, A.; Pal, R.R.; Majumder, S. Transitional Strength Under Plasma: Precise Estimations of Astrophysically Relevant Electromagnetic Transitions of Ar^{7+}, Kr^{7+}, Xe^{7+}, and Rn^{7+} Under Plasma Atmosphere. *Atoms* **2023**, *11*, 87. https://doi.org/10.3390/atoms11060087

Academic Editors: Himadri S. Chakraborty and Hari R. Varma

Received: 26 March 2023
Revised: 9 May 2023
Accepted: 16 May 2023
Published: 25 May 2023

1. Introduction

Barlow et al. [1] first observed noble gas molecules in the interstellar medium. The other detections of noble gas elements, either in diatomic [2–5] or ionic forms [6] in space at UV and IR spectra, motivate further observations of these species in the universe. It is well known that the atomic and spectroscopic processes are valuable diagnostics for plasma atmosphere in the laboratory or Astronomy. Noble gas atoms are known to be chemically inactive and require high energy to ionize. However, once ionized, their reaction rates

are rather fast. Over the years, spectroscopic properties of ionized noble gas atoms have become popular, and observers have started to detect them in space [7]. On the other hand, alkali-like ions have emerged as the standard test beds for detailed investigation of current relativistic atomic calculations due to their adequately simple but highly correlated electronic structures [8–12]. Accurate theoretical and experimental determinations of the transition line parameters and excited-state lifetimes of highly stripped ions are collaborative with the astronomer to investigate dynamics, chemical compositions, opacity, density, and temperature distributions of the distant galaxy [13], planetary nebulae, and even the entire interstellar medium [14–24]. Furthermore, one requires the accurate atomic data of different isotopes of noble gas elements to understand the production of heavy elements in the stellar medium by radiative r- and s-processes [25,26]. The data of energy spectra of moderate to high-stripped ions are required for precise astrophysical and laboratory plasma modeling. All these physical facts and figures motivate us to investigate the transition line parameters and lifetimes of septuple ionized astrophysically pertinent inert gases, such as Ar^{7+}, Kr^{7+}, Xe^{7+}, and Rn^{7+}.

In the series, Ar^{7+} is well studied in the literature. Berry et al. [27] observed 74 lines of Ar^{7+} using the beam-foil technique. In 1982, Striganov and Odintsova [28] published the observed lines of Ar^{+} through Ar^{8+}. The authors of [29–31] applied the multi-configuration Dirac–Fock (MCDF) method to calculate the autoionization spectrum, energy levels, transition rates, oscillator strengths, and lifetimes of Ar^{7+}. Saloman [32] identified the energy spectra of Ar^{+} to Ar^{17+}, which he studied from the year 2006 to 2009, employing beam foil Spectroscopy (BFS), an electron beam ion trap (EBIT), laser-excited plasmas, fusion devices, astronomical observations, and ab initio calculations with quantum electrodynamic corrections.

Similarly, krypton ion spectra were detected in the interstellar medium [33,34], the galactic disc [35], and the planetary nebulae [36]. Fine structure intervals, fine structure inversions, and core-polarization study of the Kr^{7+} ion were performed by different groups [37–39] including third-order many-body perturbation theory and Møller–Pleset perturbation theory [40,41] for the energy levels.

It is found that Cu I isoelectronic sequence ions are prominent impurities at high-temperature magnetically confined plasmas [42], and their emission spectra are observed under the spark sources [43–46] of the laser-produced plasma [47,48] and in the beam-foil excitations [49–51]. The abundance of photospheric lines of trans-iron group elements in the emission spectra of the white dwarfs opens a new way of studying their radiative transfer mechanism [52]. The presence of the spectral lines of Cu-like ions motivates more accurate determination of atomic data of the radiative properties of these ions for modeling the chemical abundances. These studies are essential for deducing the stellar parameters necessary to investigate the environmental condition of the white dwarfs. There are studies of electronic properties for Xe^{7+} using various many-body methods [53–57]. Dimitrijevc et al. [24] identified the importance of Stark broadening at the spectral lines observed in extremely metal-poor halo PNH4-1 in primordial supernova [58]. However, we study Ar^{+7}, Kr^{7+}, and Xe^{7+} here again to mitigate the lack of all-order many-body calculations or precise experiments and to estimate their spectroscopic properties under a plasma environment. Recently, one of the present authors [59] studied Xe^{7+} exclusively as a single valance system without the plasma screening effect.

Unlike other noble gas ions, studies of radon ions are rare. However, there are a few many-body calculations on Rn^{+} [60] and Rn^{2+} [61]. The observation of several forbidden lines of Kr and Xe ions in the planetary nebula NGC 7027 was reported recently [62]. For Rn^{7+}, only Migdalek [63] computed a few energy levels and oscillator strengths of allowed transitions using the Dirac–Fock method corrected by the core-polarisation effect.

The aim of this paper is to estimate (a) energies of the ground and low-lying excited states, (b) the oscillator strengths of electromagnetically allowed transitions, (c) transition probabilities of the forbidden transitions, and (d) lifetimes for a few excited states of Ar^{7+}, Kr^{7+}, Xe^{7+}, and Rn^{7+} using the relativistic coupled-cluster (RCC) method [64–66]. The

accuracies of the RCC calculations are well established by our group for different applications [67–76]. The all-order structure of electron correlation in the RCC theory has been elaborated in our earlier paper [77] and the review article by Bartlett [78]. Our special effort here is to study the plasma screening effect on the radiative transition parameters. It is obvious that the nuclear attraction to the bound electrons of atoms or ions immersed in plasma is screened by the neighboring ions and the free electrons. The essential feature to note is that the electron correlation of atomic systems in this environment is remarkably different from their corresponding isolated candidate. Therefore, the screening estimations on the transition parameters play a crucial role in the precise diagnostics of plasma temperature and density in the emitting region. In the plasma environment, the ionization potentials decrease gradually with the increasing strength of plasma screening [79] until they become zero at some critical parameter of plasma. Beyond these critical values of plasma, the states become a continuum state. The corresponding ionization potential beyond which instability occurs is known as ionization potential depression (IPD) according to the Stewart–Pyatt (SP) model [80]. Accurate determination of the IPD can infer much useful information about the plasma atmosphere, such as providing the proper equation of the state, estimating the radiate opacity of stellar plasma, internal confinement fusion plasma, etc. We have investigated the change in spectroscopic properties of Ar^{7+}, Kr^{7+}, Xe^{7+}, and Rn^{7+} in the plasma environment.

2. Theory

Precise generation of wave functions is important for accurately estimating the atomic properties of few-electron monovalent ions presented in this paper. Here, we employ a non-linear version of the well-known RCC theory, a many-body approach which exhaustively pools together correlations. Initially, we solve the Dirac–Coulomb Hamiltonian H, satisfying the eigenvalue equation $H|\Phi\rangle = E_0|\Phi\rangle$ to generate closed-shell atomic wave function under the potential of $(N-1)$ electrons where

$$H = \sum_i \left(c\alpha_i \cdot \mathbf{p}_i + (\beta_i - 1)c^2 + V_{\rm nuc}(\mathbf{r}_i) + \sum_{j<i} \left(\frac{1}{\mathbf{r}_{ij}} \right) \right).$$

Here, α_i and β are the usual Dirac matrices and $V_{nuc}(\mathbf{r_i})$ is the potential at the site of the i-th electron due to the atomic nucleus.The rest mass energy of the electron is subtracted from the energy eigenvalues. The last term corresponds to the Coulomb interaction between the i-th electron and j-th electron. A single valence reference state for the RCC calculation is generated by adding a single electron in the v-th orbital following Koopman's theorem [81]. In RCC formalism, the single valence correlated state $|\Psi_{\rm v}\rangle$ is connected with the single valence reference state $|\Phi_{\rm v}\rangle$ as

$$|\Psi_{\rm v}\rangle = e^T\{1 + S_{\rm v}\}|\Phi_{\rm v}\rangle, \quad \text{where } |\Phi_{\rm v}\rangle = a_{\rm v}^\dagger|\Phi\rangle. \tag{1}$$

The operator T deals with the excitations from core orbitals and can generate core-excited configurations from closed-shell Dirac–Fock state $|\Phi\rangle$. Whereas, $S_{\rm v}$ excites at least one electron from the valence orbital, giving rise to valence and core-valence excited configurations [64]. The operator $S_{\rm v}$ can yield the valence and core-valence excited configurations with respect to the open-shell Dirac–Fock state $|\Phi_{\rm v}\rangle$ [69]. Here, we generate single- and double-excited correlated configurations from Eq. (1). The amplitudes of these excitations are solved from the energy eigenvalue equations of the closed-shell and open-shell systems, which are $He^T|\Phi\rangle = Ee^T|\Phi\rangle$ and $H_{\rm v}e^T|\Phi_{\rm v}\rangle = E_{\rm v}e^T|\Phi_{\rm v}\rangle$, respectively [82]. In the present method, these amplitudes are solved following the Jacobi iteration scheme, which is considered all-ordered. The initial guesses of the single- and double-excitation amplitudes are made consistent with the first order of the perturbation theory [83]. In the present version of RCC theory, we also consider some important triple excitations and hence the abbreviation is used RCCSD(T).

The matrix elements of an arbitrary operator can be written as

$$\begin{aligned} O_{ki} &= \frac{\langle \Psi_k | \hat{O} | \Psi_i \rangle}{\sqrt{\langle \Psi_k | \Psi_k \rangle \langle \Psi_i | \Psi_i \rangle}} \\ &= \frac{\langle \Phi_k | \{1 + S_k^\dagger\} e^{T^\dagger} \hat{O} e^T \{1 + S_i\} | \Phi_i \rangle}{\sqrt{\langle \Phi_k | \{1 + S_k^\dagger\} e^{T^\dagger} e^T \{1 + S_k\} | \Phi_k \rangle \langle \Phi_i | \{1 + S_i^\dagger\} e^{T^\dagger} e^T \{1 + S_i\} | \Phi_i \rangle}}. \end{aligned} \tag{2}$$

The detailed derivations and explanations of the matrix elements associated with electric dipole (E_1), electric quadrupole (E_2), and magnetic dipole (M_1) transitions can be found in the literature [84]. Emission transition probabilities (s^{-1}) for the E_1, E_2, and M_1 from $|\Psi_k\rangle$ to $|\Psi_i\rangle$ state are [85]

$$A_{k\to i}^{E_1} = \frac{2.0261 \times 10^{-6}}{\lambda^3 (2J_k + 1)} S^{E_1}, \tag{3}$$

$$A_{k\to i}^{E_2} = \frac{1.12 \times 10^{-22}}{\lambda^5 (2J_k + 1)} S^{E_2}, \tag{4}$$

$$\textit{and} \qquad A_{k\to i}^{M_1} = \frac{2.6971 \times 10^{-11}}{\lambda^3 (2J_k + 1)} S^{M_1}. \tag{5}$$

where, λ is in cm and S is the square of the transition matrix elements of O (corresponding transition operator) in atomic unit of $e^2 a_0^2$(e is the charge of an electron and a_0 is the Bohr radius). The oscillator strength for the $E1$ transition is related to the corresponding transition probability (s^{-1}) with the following equation [86]

$$f_{k\to i}^{osci} = 1.4992 \times 10^{-16} A_{k\to i} \frac{g_k}{g_i} \lambda^2, \tag{6}$$

where g_k and g_i are the degeneracies of the final and initial states, respectively. The lifetime of the k-th state is calculated by considering all transition probabilities to the lower energy states (i-th) and is given by

$$\tau_k = \frac{1}{\sum_i A_{k\to i}}. \tag{7}$$

In order to incorporate the plasma screening effect on the atomic spectroscopic properties, the Dirac–Coulomb potential takes the form as

$$H_{\text{eff}}^D = H + V_{\text{eff}}^D(\mathbf{r}_i). \tag{8}$$

Here, $V_{\text{eff}}^D(\mathbf{r}_i)$ is the effective potential of the nucleus on the i-th electron due to the presence of the plasma environment. The Debye–Hückle potential is considered to examine the effect of the screening of the nuclear coulomb potential due to the presence of ions and free electrons in plasma [87,88]. In the case of a weekly interacting plasma medium, the effective potential experienced by the i-th electron is given as

$$V_{\text{eff}}^D(r_i) = \frac{Z e^{-\mu r_i}}{r_i}. \tag{9}$$

The nuclear charge Z and the Debye screening parameter μ are related to the ion density n_{ion} and plasma temperature T through the following relation

$$\mu = \left[\frac{4\pi (1 + Z) n_{ion}}{K_B T} \right]^2, \tag{10}$$

where, k_B is the Boltzmann constant. Therefore, a given value of μ represents a range of plasma conditions with different ion densities and temperatures.

3. Results and Discussions

The single-particle Dirac–Fock (DF) wavefunctions are the building blocks of the RCC calculations yielding the many-electron correlation energies and correlated wavefunctions. We calculate the bound Dirac–Hartree–Fock orbitals as accurately as possible using a sophisticated numerical approach, GRASP92 [89]. Further, we apply the basis-set expansion technique [90] in the self-consistent field approach to obtain the Gaussian-type DF orbital (GTO) used in the RCC calculations. The radial part of each basis function has two parameters, α_0, and β, as exponents [91] to be optimized. The parameters are required to optimize due to the finite size of the basis set. The exponent parameters are optimized compared to the DF bound orbitals obtained from GRASP92, discussed in detail in our old papers [12,66]. In the basis optimization method, we consider 33, 30, 28, 25, 21, and 20 basis functions for s, p, d, f, g, and h symmetries, respectively. This basis set is considered for all the ions. However, the choice of the active orbitals in the RCC calculation relies on the convergence of the correlation contribution to the closed-shell energy with the increasing number of the orbitals [66,92]. Therefore, the active orbitals for the converged correlation contribution to the closed-shell energy are found to be distinct for different ions investigated in this work.

In this article, we calculate the ionization potential of Ar^{7+}, Kr^{7+}, Xe^{7+}, and Rn^{7+} using the RCC method and compare them in Table 1 with the results published in the National Institute of Standards and Technology (NIST) [93] wherever available. The NIST estimations are considered to have the best accuracy. We find that our calculated ground state energies of Ar^{7+}, Kr^{7+}, and Xe^{7+} are in excellent agreement with NIST results, and deviations are estimated to be -0.01%, 0.45%, and -0.03%, respectively. Table 1 presents the ionization potential of the low-lying excited states of these ions with average deviations around -0.08%, 0.42%, and 0.30%, respectively. In these cases, the maximum difference is -0.23% and occurred for the $5p_{3/2}$ state of Ar^{7+}, 0.60% for $5g_{7/2,9/2}$ of Kr^{7+}, and 1.2% for $6d_{3/2,5/2}$ of Xe^{7+}.

Table 1. Comparison of our RCC ionization potential (in cm^{-1}) with NIST data and our estimations of plasma screening effect on them. Estimations for $5g$ states of Rn^{7+} were not available in the literature (a) [63]. Plasma screening strength (μ) is in a.u. unit. Energy levels are indicated as $nL(2J+1)$. The bold values indicate that beyond which the system becomes unbound.

State	NIST	$\mu = 0$	$\mu = 0.025$	$\mu = 0.05$	$\mu = 0.075$	$\mu = 0.1$
Ar^{7+}						
3s2	1,157,056	1,157,201	1,059,866	965,330	873,513	784,345
3p2	1,016,961	1,016,995	919,704	825,299	733,697	644,828
3p4	1,014,248	1,014,184	916,898	822,505	730,924	642,084
3d4	824,447	824,210	726,923	632,529	540,956	452,148
3d6	824,302	824,027	726,741	632,349	540,779	451,974
4s2	581,098	581,069	485,070	394,397	308,793	228,054
4p2	528,815	528,528	432,658	342,356	257,356	177,460
4p4	527,813	527,428	431,565	341,287	256,323	176,473
4d4	459,524	459,475	363,709	273,714	189,240	110,134
4d6	459,435	459,386	363,620	273,627	189,156	110,055
4f6	440,204	440,190	344,137	253,339	167,618	86,891
4f8	440,181	440,159	344,107	253,309	167,590	86,865
5s2	349,750	349,752	255,504	169,770	91,961	21,742
5p2	324,795	323,193	229,236	144,332	67,862	**557**
5p4	324,307	322,543	228,611	143,769	67,376	
5d4	291,782	291,699	197,867	113,352	37,637	
5d6	291,778	291,652	197,818	113,302	37,591	
5f6	281,727	281,736	187,657	102,487	25,846	
5f8	281,707	281,720	187,642	102,473	25,833	

Table 1. *Cont.*

State	NIST	$\mu = 0$	$\mu = 0.025$	$\mu = 0.05$	$\mu = 0.075$	$\mu = 0.1$
5g8	281,051	281,015	186,389	99,684	20,685	
5g10	281,037	281,015	186,380	99,676	20,678	
Kr^{7+}						
4s2	1,014,665	1,010,099	815,902	628,237	446,944	271,892
4p2	870,969	867,027	673,080	486,149	306,059	132,689
4p4	861,189	857,253	663,348	476,541	296,652	123,557
4d4	640,619	636,965	443,698	258,762	81,891	**86,678**
4d6	639,288	635,514	442,257	257,352	80,623	
5s2	524,578	523,198	331,842	152,413	**15,482**	
5p2	467,984	465,448	274,592	96,629		
5p4	464,221	461,406	270,630	92,891		
4f6	451,900	450,180	257,831	75,655		
4f8	451,934	450,186	257,837	75,660		
5d4	373,589	371,922	182,111	7230		
5d6	373,048	371,273	181,476	6635		
6s2	322,147	321,635	133,957	**34,847**		
5f6	289,666	288,637	100,173			
5f8	289,661	288,634	100,170			
5g8	281,574	281,387	92,121			
5g10	281,572	281,379	92,114			
Xe^{7+}						
5s2	854,769	854,995	564,858	286,731	20,272	
5p2	738,302	737,059	447,391	170,643	**93,515**	
5p4	719,717	718,263	428,759	152,487		
4f6	589,608	588,730	297,599	16,588		
4f8	589,058	588,088	296,970	16,085		
5d4	544,881	543,506	255,203	**17,518**		
5d6	541,953	540,549	252,295			
6s2	459,272	455,364	170,155			
6p2	411,391	406,318	121,973			
6p4	403,996	398,801	114,717			
5f6	357,190	356,376	70,683			
5f8	356,751	355,922	70,245			
6d4	327,344	323,450	41,320			
6d6	325,975	322,176	40,102			
7s2	289,473	276,902	**451**			
5g8	284,501	283,609				
5g10	284,501	283,617				
Rn^{7+}	(a)					
6s2	834,624	839,362	377,923	**63,552**		
6p2	712,821	718,015	257,667			
6p4	661,071	665,627	205,616			
5f6	536,092	531,079	69,545			
5f8	534,720	529,291	68,106			
6d4	498,636	501,235	43,424			
6d6	491,240	493,699	36,116			
7s2	446,847	445,577	**8041**			
7p2	397,883	398,535				
7p4	377,435	377,332				
5g8		287,997				
5g10		288,252				

Our calculated energies agree well with estimations by Fischer et al. [31], who computed energy levels of Ar^{7+} using the core polarization effect on the Dirac–Hartree–Fock (CP-DHF) theory. Cheng and Kim [37] tabulated the energy levels of Kr^{7+} from the relativistic Hartree–Fock (RHF) calculations. As expected, our RCC calculated results are found to be in better agreement with the NIST values. For Rn^{7+}, we have not found any

experimental measurement in the literature nor NIST compiled values. Only one theoretical calculation based on the CP-DHF method by [63] is available with the average deviation of IP being 0.66% from our calculations.

The percentage of electron correlation correction, i.e., $\frac{(\text{RCC-DF})\times 100\%}{\text{DF}}$ in IP of the ground state monotonically increases from Ar^{7+} to Rn^{7+} with the values 0.39%, 0.52%, 1.81%, and 1.87%, respectively.

Now, we investigate the impact of the plasma screening potential on the energy levels of the considered ions. Table 1 shows that IP monotonically decreases with the increase in the μ value. The bold values for each ion in the table represent the limiting case beyond which the system becomes unbound. Figure 1 presents the plasma screening contribution in IP for a few low-lying states, such as ground state $S_{1/2}$, excited $P_{1/2,3/2}$, and $D_{3/2,5/2}$ states of Ar^{7+}, Kr^{7+}, Xe^{7+}, and Ra^{7+} ions. The panels of the figure show the plasma screening contribution increases from the ground to higher excited states, as the latter states are less bound by the Coulomb attraction. For Xe^{7+} and Rn^{7+}, we could plot the effect up to a certain value of μ as most of the states become continuum states beyond that. We observe that the plasma screening effect is practically strong for fine structure levels for Ar^{7+} and Kr^{7+} ions and weak for Xe^{7+}, and Ra^{7+} ions.

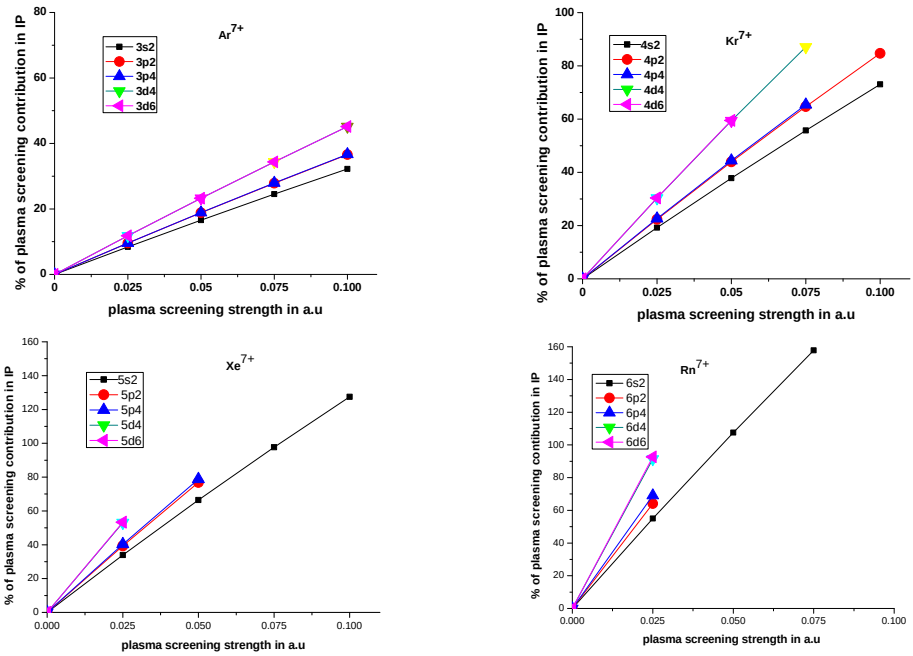

Figure 1. The plasma contribution in IP of low-lying septuple ionized atoms: % variation of IP with plasma screening strength. Energy levels are indicated as $nL(2J+1)$. Results are calculated from $\frac{\text{IP}_{\mu=0}-\text{IP}_{\mu>0}}{\text{IP}_{\mu=0}} \times 100$.

We present the electric dipole matrix elements for the ions in the plasma medium in Table 2. The table also displays our computed DF values of the matrix elements to reveal the correlation contributions. The separate presentation of the DF and RCC values over the span of the plasma screening parameter, μ, in the table is an intentional move. Here, we want to highlight that the plasma screening impacts the DF and the RCC correlation parts differently. In the case of Ar^{7+}, the average changes in the matrix element due to the increasing values of the plasma screening parameter are less than 1%. However, Figure 2 shows significant changes for $3s_{1/2} \rightarrow 4p_{1/2,3/2}$ and $3s_{1/2} \rightarrow 5p_{1/2,3/2}$ for finite values of μ, especially for $\mu = 0.05$. This is true for any $n\,^2S_{1/2} \rightarrow n'\,^2P_{1/2,3/2}$ of this ionic series. However, apart from such a few transitions, the plasma effects lie between 1 % and 2 % for most of the other transitions in the series. Table 2 shows that the average correlations (for the non-plasma environment) in the transition amplitudes for Ar^{7+}, Kr^{7+}, Xe^{7+}, and Rn^{7+} are 0.3858%, 4.0831%, 7.6074%, and 11.6379% apart from the $4d_{3/2} \rightarrow 5f_{5/2}$ transition where the correlation is 67.11%.

Table 2. Our DF and RCC matrix element (a.u.), in length gauge, of electric dipole ($E1$) transitions in plasma medium. Energy levels are indicated as $nL(2J+1)$.

	$\mu = 0$		$\mu = 0.025$		$\mu = 0.05$		$\mu = 0.075$		$\mu = 0.1$	
Ar^{7+}										
Transitions	DF	RCC	DF	RCC	DF	RCC	DF	RCC	DF	RCC
3s2→3p2	0.9617	0.9341	0.9623	0.9346	0.9638	0.9390	0.9663	0.9405	0.9697	0.9436
3s2→3p4	1.3619	1.3228	1.3626	1.3236	1.3648	1.3299	1.3683	1.3317	1.3732	1.3355
3s2→4p2	0.2002	0.2093	0.1999	0.2089	0.1989	0.2210	0.1973	0.2181	0.1950	0.2164
3s2→4p4	0.2770	0.2898	0.2765	0.2893	0.2751	0.3059	0.2728	0.3028	0.2698	0.3012
3s2→5p2	0.1011	0.1062	0.1006	0.1057	0.0992	0.0995	0.0972	0.1105	0.0944	0.1007
3s2→5p4	0.1397	0.1470	0.1390	0.1463	0.1372	0.1215	0.1345	0.1541	0.1307	0.1528
4s2→4p2	1.8958	1.8813	1.8996	1.8851	1.9105	1.9059	1.9284	1.8987	1.9537	1.9012
4s2→4p4	2.6827	2.6622	2.6879	2.6675	2.7033	2.7006	2.7286	2.6857	2.7644	2.6844
3p2→4s2	0.3604	0.3646	0.3608	0.3649	0.3619	0.3419	0.3637	0.3437	0.3661	0.3432
3p4→4s2	0.5172	0.5231	0.5178	0.5236	0.5193	0.4898	0.5219	0.4943	0.5253	0.4952
3p2→5s2	0.1237	0.1269	0.1240	0.1271	0.1246	0.1275	0.1252	0.1144	0.1253	0.1274
3p4→5s2	0.1771	0.1816	0.1775	0.1819	0.1783	0.2021	0.1792	0.1653	0.1793	0.1659
3p2→3d4	1.3534	1.3174	1.3547	1.3186	1.3583	1.3207	1.3642	1.3218	1.3725	1.3305
3p4→3d4	0.6060	0.5899	0.6066	0.5905	0.6082	0.5916	0.6109	0.5918	0.6146	0.5956
3p4→3d6	1.8184	1.7700	1.8201	1.7720	1.8250	1.7736	1.8330	1.7750	1.8442	1.7795
3p2→4d4	0.3857	0.3957	0.3842	0.3942	0.3800	0.3925	0.3730	0.3926	0.3629	0.3551
3p4→4d4	0.1756	0.1801	0.1750	0.1794	0.1731	0.1770	0.1699	0.1791	0.1654	0.1645
3p4→4d6	0.5262	0.5394	0.5242	0.5375	0.5185	0.5321	0.5091	0.5372	0.4956	0.5357
4p2→4d4	2.7891	2.7687	2.7966	2.7761	2.8181	2.7737	2.8536	2.7737	2.9038	2.8032
4p4→4d4	1.2496	1.2405	1.2529	1.2438	1.2626	1.2470	1.2785	1.2420	1.3010	1.2498
4p4→4d6	3.7490	3.7217	3.7590	3.7316	3.7880	3.7880	3.8357	3.7255	3.9033	3.7279
3d4→4p2	0.5411	0.5434	0.5426	0.5449	0.5470	0.5616	0.5542	0.5407	0.5644	0.5701
3d4→4p4	0.2395	0.2406	0.2402	0.2412	0.2487	0.2450	0.2454	0.2395	0.2499	0.2530
3d6→4p4	0.7193	0.7225	0.7213	0.7244	0.7271	0.7193	0.7368	0.7201	0.7504	0.7184
3d4→4f6	1.7707	1.7378	1.7705	1.7377	1.7702	1.7384	1.7691	1.7401	1.7663	1.7778
3d6→4f6	0.4734	0.4671	0.4734	0.4646	0.4733	0.4649	0.4730	0.4653	0.4722	0.4658
3d6→4f8	2.1172	2.078	2.1171	2.0779	2.1166	2.0793	2.1154	2.0768	2.1121	2.0799
4d4→4f6	3.1546	3.1495	3.1686	3.1634	3.2100	3.1508	3.2796	3.1504	3.3822	3.1414
4d6→4f6	0.8430	0.8416	0.8468	0.8454	0.8578	0.8420	0.8764	0.8419	0.9087	0.8423
4d6→4f8	3.7706	3.7644	3.7874	3.7812	3.7652	3.7644	3.9201	3.7778	4.0427	3.7790
Kr^{7+}										
	DF	RCC	DF	RCC	DF	RCC	DF	RCC	DF	RCC
4s2→4p2	1.1348	1.0794	1.1363	1.1017	1.1405	1.1223	1.1475	1.1088	1.1575	1.1245
4s2→4p4	1.6095	1.5314	1.6115	1.5632	1.6175	1.5900	1.6275	1.5724	1.6416	1.6085
4s2→5p2	0.1488	0.1655	0.1479	0.1584	0.1451	0.1537				
4s2→5p4	0.1812	0.2057	0.1799	0.1944	0.1761	0.1839				
4p2→4d4	1.7539	1.6812	1.7569	1.7412	1.7657	1.7506	1.7804	1.7422		
4p4→4d4	0.7940	0.7616	0.7954	0.7734	0.7995	0.7836	0.8064	0.7771		
4p4→4d6	2.3818	2.2847	2.3860	2.3218	2.3984	2.3511	2.4190	2.3301		
4p2→5s2	0.4884	0.4934	0.4894	0.4892	0.4925	0.4838				
4p4→5s2	0.7316	0.7379	0.7331	0.7325	0.7377	0.7272				
4p2→6s2	0.1655	0.1686	0.1654	0.1664	0.1646	0.1624				
4p4→6s2	0.2447	0.2486	0.2445	0.2460	0.2427	0.2424				
4d4→4f6	2.8243	2.7466	2.8340	2.7759	2.8623	2.7985				
4d6→4f6	0.7565	0.7358	0.7591	0.7436	0.7668	0.7499				
4d4→5p2	1.1740	1.1630	1.1809	1.1776	1.2015	1.1742				
4d4→5p4	0.5090	0.5124	0.5120	0.5107	0.5212	0.5168				
4d6→5p4	1.5415	1.5522	1.5507	1.5464	1.5786	1.5435				
4d6→4f8	3.3836	3.2916	3.3953	3.3257	3.4297	3.3529				
4d4→5f6	0.0596	0.0427	0.0582	0.0445						
4d6→5f6	0.0133	0.0091	0.0175	0.0089						
4d6→5f8	0.0592	0.0418	0.0779	0.0394						
4f6→5g8	3.8576	3.7993	3.8688	3.8112						
4f8→5g8	0.7422	0.7311	0.7444	0.7340						
4f8→5g10	4.3914	4.3256	4.4042	4.3380						
4f6→5d4	2.0421	2.0387	2.0728	2.0318	2.1683	2.0704				
4f6→5d6	0.5430	0.5420	0.5512	0.5401	0.5766	0.5498				
4f8→5d6	2.4274	2.4232	2.4641	2.4137	2.5780	2.4567				
5p2→5d4	3.1683	3.1275	3.1867	3.1373	3.2401	3.1494				
5p4→5d4	1.4407	1.4226	1.4489	1.4271	1.4728	1.4325				
5p4→5d6	4.3172	4.2629	4.3417	4.2781	4.4131	4.2912				
5p2→6s2	1.0220	1.0239	1.0277	1.0215						
5p4→6s2	1.5278	1.5310	1.5347	1.5276						

Table 2. *Cont.*

	$\mu = 0$		$\mu = 0.025$		$\mu = 0.05$		$\mu = 0.075$		$\mu = 0.1$	
Xe^{7+}	DF	RCC	DF	RCC	DF	RCC	DF	RCC	DF	RCC
5s2→5p2	1.3758	1.1736	1.3791	1.1769	1.3889	1.1866				
5s2→5p4	1.9516	1.6705	1.9562	1.6752	1.9700	1.6890				
5p2→5d4	2.1135	1.8629	2.1197	1.8697						
5p4→5d4	0.9768	0.8646	0.9799	0.8679						
5p4→5d6	2.9252	2.5911	2.9344	2.6011						
5p2→6s2	0.5866	0.6026	0.5893	0.6046						
5p4→6s2	0.9449	0.9582	0.9494	0.9619						
4f6→5d4	1.7952	1.5958	1.8177	1.6155						
4f6→5d6	0.4761	0.4237	0.4822	0.4291						
4f8→5d6	2.1392	1.9075	2.1663	1.9313						
4f6→5g8	1.8079	1.5869	1.7885	1.5731						
4f8→5g8	0.3495	0.3073	0.3457	0.3046						
4f8→5g10	2.0684	1.819	2.0462	1.8032						
5d4→5f6	2.9732	2.8328	2.9687	2.8347						
5d6→5f6	0.8050	0.7670	0.8040	0.7676						
5d6→5f8	3.5922	3.4233	3.5876	3.4252						
6s2→6p2	2.7436	2.5326	2.5640	2.5931						
6s2→6p4	3.3346	3.5052	3.6133	3.6569						
6p2→6d4	3.7253	3.5930	3.7520	3.6089						
6p4→6d4	1.7277	1.6725	1.7399	1.6762						
6p4→6d6	5.1635	4.9966	5.1994	5.0147						
5f6→5g8	5.5926	5.3626								
5f6→5g8	1.0772	1.0330								
5f8→5g10	6.3725	6.1114								
Rn^{7+}	DF	RCC	DF	RCC	DF	RCC	DF	RCC	DF	RCC
6s2→6p2	1.4159	1.1344	1.4210	1.1414						
6s2→6p4	1.9902	1.6147	1.9969	1.6264						
6p2→7s2	0.6184	0.6284	0.6189	0.6678						
6p4→7s2	1.2512	1.2162	1.2657	1.2024						
6p2→6d4	2.0887	1.7562	2.0978	1.7629						
6p4→6d4	1.0493	0.8953	1.0556	0.9008						
6p4→6d6	3.1200	2.6596	3.1380	2.6691						
5f6→6d4	2.3362	2.0900	2.3794	2.0911						
5f6→6d6	0.6118	0.5500	0.6236	0.5478						
5f8→6d6	2.7709	2.4962	2.8234	2.4931						
5f6→5g8	2.7042	2.3829								
5f8→5g8	0.5263	0.4650								
5f8→5g10	3.1174	2.7455								
7s2→7p2	2.5750	2.4195								
7s2→7p4	3.5648	3.3636								
6d4→7p2	2.0098	1.9415								
6d4→7p4	0.7525	0.7381								
6d6→7p4	2.4112	2.3331								

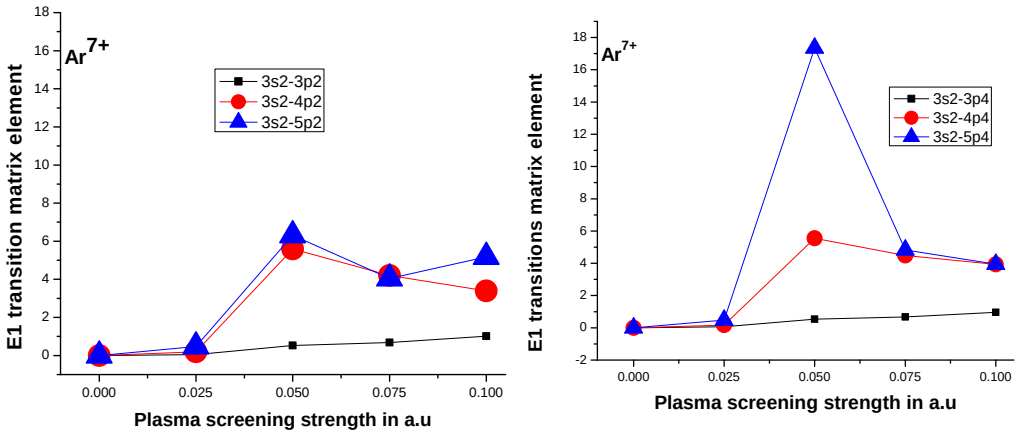

Figure 2. The contribution of plasma screening in E1 matrix elements of Ar^{7+} of transitions ${}^2S_{1/2} \rightarrow {}^3P_{1/2,3/2}$. The figures display % variation of the E1 matrix elements vs. plasma screening strength.

For observational astronomy and laboratory spectroscopy, we present a tabulation of a list of our computed oscillator strengths ($f_{\mathrm{R\,CC}}$) of $E1$ transitions along with their previously reported theoretical and experimental values in Table 3. Most of the transitions fall in the far and mid-UV regions of the electromagnetic spectrum. f_{RCC} is calculated using the RCC transition amplitudes in length gauge [94] form presented in Table 2 and the NIST [93] wavelengths, wherever available (in the case of Rn^{7+}, our computed RCC wavelengths are used). The ratios between the length and velocity gauge amplitudes of our calculated $E1$ transitions are also displayed in table to show the accuracy of our RCC wavefunctions, which is close to unity for all the cases, confirming the accuracy of our correlated atomic wavefunctions. However, we find that the ratio is almost two for $^2F \rightarrow {}^2D$ transitions of Xe^{7+} and Rn^{7+}. A point to note is that this disagreement is also available in the ratio at the DF level, where we also employed the numerically accurate GRASP92 Code [89]. One of the reasons for this outcome is due to the strong correlation effect from the d- and f-states, as so in similar alkali systems [95]. In addition, the consistency of the accuracy of our calculations can be drawn from the approximate consistency of the ratios 3:2:1 among the transition matrix estimations of $^2P_{3/2} \rightarrow {}^2D_{5/2}$: $^2P_{1/2} \rightarrow {}^2D_{3/2}$: $^2P_{3/2} \rightarrow {}^2D_{3/2}$ [96].

The $E1$ Oscillator strengths for Ar^{7+} are well studied in the literature [31,97–105], and they are in good agreement with our estimations based on the correlation exhaustive RCC method. Table 3 shows that the same is true for Kr^{7+}. For Ar^{7+}, our calculations for f_{RCC} are almost as accurate as those found from other sophisticated theoretical approaches, such as the relativistic many-body perturbation theory [102], and for the most latest theoretical results employing the multiconfigurational Dirac–Hartree–Fock approximation [31]. To the best of our knowledge, in the case of Kr^{7+}, we could not find any correlation-exhaustive many-body result of $E1$ transition. There have been experiments, mostly using beam-foil experiments, on the $E1$ transition from the ground state to the first excited states of Ar^{7+} [97], and Kr^{7+} [49–51,106,107]. Our estimations are well within the uncertainty limit of the latest experiments. We also see that some of the old calculations either underestimate or overestimate the oscillator strength values due to non-appropriate considerations of correlations and relativistic effects.

Table 3. Our RCC oscillator strengths of electric dipole transitions. We compare our results with other estimations available in the recent literature (experimental endeavors are highlighted with "exp" subscript). Our results ("RCC") are obtained using the RCC calculations, except NIST wavelengths are used for $\mu = 0$ wherever available. Transition states are designated with the outermost orbital followed by $(2J + 1)$ of the state. Values at the parenthesis in the second column are ratios between length- and velocity-gauged dipole matrix elements.

	$\mu = 0$		$\mu = 0.025$	$\mu = 0.050$	$\mu = 0.075$	$\mu = 0.1$
Transition	***RCC***	**Other**				
Ar^{7+}						
3s2 → 3p2	0.1857 (0.99)	0.183 $(4)^{a_1}_{exp}$, 0.188 ^{b_1}, 0.193 ^{c_1}, 0.186 ^{d_1}, 0.1864 ^{e_1}, 0.185 ^{f_1,i_1}, 0.187 ^{g_1}, 0.196 ^{h_1}	0.1859	0.1875	0.1878	0.1887
3s2 → 3p4	0.3795 (0.99)	0.398(10) $^{a_1}_{exp}$, 0.385 ^{b_1}, 0.394 ^{c_1}, 0.381 ^{d_1,g_1}, 0.3811 ^{e_1}, 0.379 ^{f_1}, 0.401 ^{h_1}, 0.378 ^{i_1}	0.3804	0.3837	0.3840	0.3854
3s2 → 4p2	0.0418 (1.00)	0.0414 ^{b_1}, 0.0401 ^{c_1}, 0.0376 ^{d_1} 0.0415 ^{e_1}, 0.0385 ^{h_1}, 0.0432 ^{i_1}	0.0416	0.0462	0.0445	0.0432
3s2 → 4p4	0.0803 (1.00)	0.0829 ^{b_1}, 0.0766 ^{c_1}, 0.0751 ^{d_1}, 0.0798 ^{e_1}, 0.0739 ^{h_1}, 0.0836 ^{i_1}	0.0793	0.0877	0.0859	0.0838
3s2 → 5p2	0.0143 (0.98)	0.0146 ^{b_1,e_1}	0.0141	0.0123	0.0149	0.0121
3s2 → 5p4	0.0271 (1.00)	0.0292 ^{b_1}, 0.0284 ^{e_1}	0.0270	0.0184	0.0291	0.0278
4s2 → 4p2	0.2810 (1.01)	0.2821 ^{e_1}, 0.2824 ^{i_1}	0.2829	0.2871	0.2816	0.2777
4s2 → 4p4	0.5736 (1.01)	0.5755 ^{e_1}, 0.5759 ^{i_1}	0.5782	0.5883	0.5748	0.5645
3p2 → 4s2	0.0880 (1.00)	0.0876 ^{e_1}, 0.0884 ^{i_1}	0.0879	0.0765	0.0763	0.0760
3p4 → 4s2	0.0900 (1.01)	0.0896 ^{e_1}, 0.08947 ^{i_1}	0.0899	0.0780	0.0783	0.0783
3p2 → 5s2	0.0163 (1.01)	0.0161 ^{e_1}	0.0163	0.0162	0.0128	0.0154
3p4 → 5s2	0.0166 (1.01)	0.0164 ^{e_1}	0.0166	0.0202	0.0133	0.0130

Table 3. *Cont.*

		$\mu = 0$	$\mu = 0.025$	$\mu = 0.050$	$\mu = 0.075$	$\mu = 0.1$
Transition	***RCC***	**Other**				
3p2 → 3d4	0.5074 (0.96)	0.532 ^{c_1}, 0.5097 ^{e_1}, 0.5074 ^{g_1} 0.508 ^{i_1}, 0.47 ^{j_1}	0.5091	0.5107	0.5115	0.5180
3p4 → 3d4	0.0502 (0.96)	0.0527 ^{c_1}, 0.0504 ^{e_1}, 0.0501 ^{g_1} 0.0502 ^{i_1}, 0.046 ^{j_1}	0.0503	0.0505	0.0505	0.0512
3p4 → 3d6	0.4556 (0.96)	0.475 ^{c_1}, 0.4539 ^{e_1}, 0.4517 ^{g_1} 0.452 ^{i_1}, 0.42 ^{j_1}	0.4534	0.4542	0.4549	0.4571
3p2 → 4d4	0.1326 (1.05)	0.1310 ^{e_1}, 0.1344 ^{i_1}	0.1312	0.1291	0.1275	0.1024
3p4 → 4d4	0.0137 (1.03)	0.0135 ^{e_1}, 0.0136 ^{i_1}	0.0135	0.0131	0.0132	0.0109
3p4 → 4d6	0.1226 (1.03)	0.1212 ^{e_1}, 0.1228 ^{i_1}	0.1214	0.1180	0.1187	0.1159
4p2 → 4d4	0.8067 (0.95)	0.8085 ^{i_1}	0.8070	0.8020	0.7930	0.8035
4p4 → 4d4	0.0798 (0.98)	0.0796 ^{i_1}	0.0797	0.0798	0.0786	0.0787
4p4 → 4d6	0.7192 (0.98)	0.7177 ^{i_1}	0.7185	0.7215	0.7079	0.7009
3d4 → 4p2	0.0663 (0.98)	0.0657 ^{e_1}, 0.0663 ^{i_1}	0.0663	0.0695	0.0630	0.0678
3d4 → 4p4	0.0130 (1.00)	0.0129 ^{e_1}, 0.0131 ^{i_1}	0.0130	0.0133	0.0124	0.0134
3d6 → 4p4	0.0784 (0.97)	0.0778 ^{e_1}, 0.0786 ^{i_1}	0.0784	0.0762	0.0747	0.0720
3d4 → 4f6	0.8812 (1.00)	0.8776 ^{i_1}	0.8777	0.8702	0.8584	0.8762
3d6 → 4f6	0.0424 (1.00)	0.0418 ^{i_1}	0.0418	0.0415	0.0409	0.0401
3d6 → 4f8	0.8397 (1.00)	0.8360 ^{i_1}	0.8364	0.8297	0.8149	0.7796
Kr^{7+}						
4s2 ⟶ 4p2	0.2543 (1.00)	0.25(1) $^{a_2,f_2}_{exp}$, 0.24(2) $^{b_2}_{exp}$, 0.246 ^{c_2}, 0.2781 ^{d_2}, 0.278 ^{e_2}, 0.28 ^{g_2}, 0.2578 ^{h_2}, 0.220 ^{i_2}, 0.2448 ^{j_2}	0.2633	0.2718	0.2705	0.2673
4s2 ⟶ 4p4	0.5466 (0.97)	0.53(2) $^{a_2}_{exp}$, 0.47(4) $^{b_2}_{exp}$, 0.526 ^{c_2}, 0.5965 ^{d_2}, 0.60 ^{e_2}, 0.59 (9) $^{f_2}_{exp}$, 0.59 ^{g_2}, 0.554 ^{h_2}, 0.473 ^{i_2} 0.5265 ^{j_2}	0.5661	0.5825	0.5833	0.5829
4s2 ⟶ 5p2	0.0227 (1.01)	0.0176 ^{d_2}	0.0206	0.0191		
4s2 ⟶ 5p4	0.0354 (1.00)	0.0265 ^{d_2}	0.0313	0.0275		
4p2 → 5s2	0.1281 (1.02)	0.1212 ^{d_2}	0.1261	0.1187		
4p4 → 5s2	0.1392 (1.02)	0.1321 ^{d_2}	0.1351	0.1302		
4p2 → 4d4	0.9888 (1.00)	1.057 ^{d_2}	1.0562	1.0583	1.1068	
4p4 → 4d4	0.0972 (1.00)	0.1038 ^{d_2}	0.0998	0.1015	0.1045	
4p4 → 4d6	0.8796 (1.00)	0.9395 ^{d_2}	0.9051	0.9200	0.9480	
4p2 → 6s2	0.0237 (1.06)	0.0208 ^{d_2}	0.0227	0.0181		
4p4 → 6s2	0.0253 (1.07)	0.0220 ^{d_2}	0.0243	0.0197		
4d4 → 4f6	1.0811 (0.98)	1.126 ^{d_2}	1.0876	1.0890		
4d6 → 4f6	0.0514 (0.98)	0.0535 ^{d_2}	0.0508	0.0509		
4d6 → 4f8	1.0277 (0.98)	1.0700 ^{d_2}	1.0326	1.0340		
4d4 → 5p2	0.1828 (1.00)	0.1784 ^{d_2}	0.1781	0.1697		
4d4 → 5p4	0.0352 (1.03)	0.0344 ^{d_2}	0.0345	0.0329		
4d6 → 5p4	0.2135 (1.00)	0.2088 ^{d_2}	0.2078	0.1984		
4d4 → 5f6	0.0001 (1.09)	0.0001 ^{d_2}	0.0005			
4f6 → 5d4	0.1647 (0.98)	0.1638 ^{d_2}	0.1582	0.1485		
4f6 → 5d6	0.0117 (0.98)	0.0117 ^{d_2}	0.0113	0.0106		
4f8 → 5d6	0.1759 (0.98)	0.1750 ^{d_2}	0.1689	0.1582		
4f6 → 5g8	1.2447 (1.00)	1.261 ^{d_2}	1.2185			
4f8 → 5g8	0.0346 (1.00)	0.0350 ^{d_2}	0.0339			
4f8 → 5g10	1.2103 (1.00)	1.226 ^{d_2}	1.1841			
5p2 → 5d4	1.4023 (1.00)	1.401 ^{d_2}	1.3825	1.3467		
5p4 → 5d4	0.1393 (1.01)	0.1383 ^{d_2}	0.1369	0.1335		
5p4 → 5d6	1.2582 (1.01)	1.249 ^{d_2}	1.2391	1.2062		
4d6 → 5f6	0.00002 (0.28)	0.00003 ^{d_2}	0.00001			
4d6 → 5f8	0.0003 (0.29)	0.0007 ^{d_2}	0.0003			
5p2 → 6s2	0.2322 (1.07)	0.2023 ^{d_2}	0.2229			
5p4 → 6s2	0.2529 (1.08)	0.2179 ^{d_2}	0.2422			
Xe^{7+}						
5s2 → 5p2	0.2436 (1.01)	0.294 ^{a_3}, 0.234 ^{b_3}, 0.242 ^{c_3} 0.253 ^{d_3}, 0.237 ^{e_3}, 0.237 ^{f_3} 0.232 ^{g_3}, 0.223 ^{h_3}, 0.232 ^{i_3}	0.2471	0.2482		

Table 3. *Cont.*

		$\mu = 0$	$\mu = 0.025$	$\mu = 0.050$	$\mu = 0.075$	$\mu = 0.1$
Transition	***RCC***	**Other**				
5s2 → 5p4	0.5724 (1.01)	0.697 [a3], 0.550 [b3], 0.569 [c3] 0.596 [d3], 0.560 [e3], 0.563 [f3], 0.543 [g3], 0.522 [h3], 0.537 [i3]	0.5801	0.5816		
5p2 →5d4	1.0195 (1.02)	1.189 [a3], 0.977 [b3], 1.020 [c3] 1.025 [d3], 1.003 [e3], 1.000 [f3] 1.057 [i]	1.0204			
5p4 →5d4	0.0992 (1.02)	0.095 [b3], 0.089 [c3], 0.099 [d3] 0.097 [e3], 0.097 [f3], 0.095 [i3]	0.0993			
5p4 →5d6	0.9064 (1.02)	0.523 [a3], 0.868 [b3], 0.904 [c3] 0.907 [d3], 0.889 [e3], 0.886 [f3] 0.875 [i3]	0.9066			
5p2 → 6s2	0.1539 (1.05)	0.160 [c3], 0.156 [d3], 0.155 [e3] 0.153 [f3], 0.199 [i3]	0.1539			
5p4 → 6s2	0.1816 (1.05)	0.188 [c3], 0.186 [d3], 0.184 [e3] 0.182 [f3], 0.186 [i3]	0.1817			
4f6 → 5d4	0.0577 (2.35)	0.130 [a3], 0.058 [b3], 0.060 [i3]	0.0560			
4f6 → 5d6	0.0043 (2.12)	0.0044 [b3]	0.0042			
4f8 → 5d6	0.0651 (2.19)	0.075 [a3], 0.065 [b3], 0.068 [i3]	0.0633			
4f6 → 5g8	0.3890 (1.02)	0.3646 [b3], 0.354 [i3]				
4f8 → 5g8	0.0109 (1.02)	0.0102 [b3]				
4f8 → 5g10	0.3826 (1.02)	0.3595 [b3], 0.343 [i3]				
5d4 → 5f6	1.1437 (1.04)	1.099 [i3]	1.1259			
5d6 → 5f6	0.0550 (1.04)	0.052 [i3]	0.0813			
5d6 → 5f8	1.0981 (1.04)	1.032 [i3]	1.0812			
5f6 → 5g8	1.0583 (0.99)	1.071 [i3]				
5f8 → 5g8	0.0293 (0.99)	0.030 [i3]				
5f8 → 5g10	1.0246 (0.99)	1.035 [i3]				
6s2 → 6p2	0.4778 (1.13)		0.4921			
6s2 → 6p4	1.0555 (1.13)		1.1260			
6p2 → 6d4	1.6248 (1.11)		1.5953			
6p4 → 6d6	1.4527 (1.11)		1.4249			
6p4 → 6d4	0.1601 (1.11)		0.1566			
Rn^{7+}						
6s2 → 6p2	0.2372 (1.00)	0.234 [a4]	0.2379			
6s2 → 6p4	0.6880 (1.02)	0.689 [a4]	0.6922			
6p2 → 7s2	0.1634 (1.06)	0.173 [a4]				
6p4 → 7s2	0.2472 (1.07)	0.259 [a4]				
6p2 →6d4	1.0154 (1.01)	1.059 [a4]	1.0113			
6p4 →6d4	0.1001 (1.01)	0.103 [a4]	0.0999			
6p4 →6d6	0.9234 (1.01)	0.956 [a4]	0.9170			
5f6 → 6d4	0.0660 (2.13)	0.0753 [a4]	0.0578			
5f8 → 6d6	0.0842 (1.83)	0.0981 [a4]	0.0755			
5f6 → 6d6	0.0057 (1.73)	0.0069 [a4]	0.0051			
5f6 → 5g8	0.6982 (1.00)					
7s2 → 7p2	0.4182 (1.11)	0.414 [a4]				
7s2 → 7p4	1.1727 (1.12)	1.126 [a4]				
6d4 → 7p2	0.2940 (1.05)	0.292 [a4]				
6d4 → 7p4	0.0513 (1.04)	0.052 [a4]				
6d6 → 7p4	0.3207 (1.05)	0.33 [a4]				

$a_1 \Longrightarrow$ Beam-foil technique [97]; $b_1 \Longrightarrow$ calculations are based on high level methods such as the R-matrix method and asymptotic techniques developed by Seaton [98]; $c_1 \Longrightarrow$ Single Configuration Interaction Hartree–Fock method using a pseudopotential [99]; $d_1 \Longrightarrow$ non-relativistic WKB approaches (Klein–Gordon dipole matrix) [100]; $e_1 \Longrightarrow$ single configuration Dirac–Fock method [101]; $f_1 \Longrightarrow$ relativistic many-body perturbation theory [102]; $g_1 \Longrightarrow$ realistic model potential [103]; $h_1 \Longrightarrow$ relativistic Hartree–Fock method [104]; $i_1 \Longrightarrow$ multiconfiguration Dirac–Hartee-Fock approximation. [31]; $j_1 \Longrightarrow$ relativistic effective orbital quantum number [105]; $a_2 \Longrightarrow$ jointly analyzed decay curves: beam-foil [106]; $b_2 \Longrightarrow$ multiexponential fits: beam-foil [106]; $c_2 \Longrightarrow$ Non-Relativistic Multi Configuration Hartree–Fock approximation [108]; $d_2 \Longrightarrow$ relativistic Hartree–Fock [37]; $e_2 \Longrightarrow$ Hartree-Fock oscillator strength using the Dirac correction factor [109]; $f_2 \Longrightarrow$ Arbitrarily Normalized Decay curve method for cascade-correction in beam-foil [107]; $g_2 \Longrightarrow$ Hartree–Fock with relativistic correction [110]; $h_2 \Longrightarrow$ semi-empirical Coulomb approximation [111]; $i_2 \Longrightarrow$ model potential [112]; $j_2 \Longrightarrow$ Hartree-Slater method [23]; $a_3 \Longrightarrow$ RPTMP [57]; $b_3 \Longrightarrow$ RMBPT(3) [55]; $c_3 \Longrightarrow$ DF+CP [54]; $d_3 \Longrightarrow$ DX+CP method with SCE model potential [54]; $e_3 \Longrightarrow$ DX+CP method with CAFEGE model potential [54]; $f_3 \Longrightarrow$ DX+CP method with HFEGE model potential [54]; $g_3 \Longrightarrow$ CIDF method with integer occupation number [56]; $h_3 \Longrightarrow$ CIDF(q) method with non-occupation number [56]; $i_3 \Longrightarrow$ HFR+CP method [53]; $a_4 \Longrightarrow$ relativistic core-polarization corrected Dirac–Fock method (DF+CP) [63].

Over the last two decades, a few of the low-lying $E1$ transitions of Xe^{7+} are estimated using core-polarization or model potential as an effective means of correlation calculations, apart from third-order perturbation calculations [55]. It is known that our RCC method is an all-order extension of many-body perturbation theory [83]. Further, it includes most of the correlation features, including core correlation, pair correlation, and higher order correlation effects [69] for a given level of excitation. For Rn^{7+}, we find only one theoretical endeavor [63] using the model potential. The presence of d- and f-orbitals for Xe^{7+} and Rn^{7+} ions in the core makes these two ions highly correlated. Because of the large atomic number and highly stripped configurations, we expect a strong relativistic effect in their spectroscopy. Therefore, it is necessary to do relativistic ab initio correlation exhaustive calculations for them and our computations exactly mitigate that requirement. In Table 3, we also present the effect of the plasma atmosphere on the oscillator strengths for observational and laboratory spectroscopy. The oscillator strengths for $\mu > 0$ are calculated using the $E1$ matrix elements presented in Table 2 and the corresponding transition wavelengths computed from RCC theory. The table exhibits the significant effects of plasma screening parameters on the oscillator strengths.

Tables 4 and 5 present transition probabilities for the relatively strong forbidden transitions governed by the electric quadruple ($E2$) and the magnetic dipole ($M1$) moments. Similar to oscillator strength in Table 3, here we use NIST wavelengths for the transition probability wherever available. For Rn^{7+}, we use the RCC calculated transition wavelengths. We do not find any estimation of the forbidden transitions in the literature of this ionic series which fall either in the ultraviolet or in the near infra-red regions of the electromagnetic spectrum. Transitions falling in the ultraviolet region are significant in astronomical observation and plasma research [113–116]. In comparison, the infra-red transitions have applications in astronomy using space-based telescopes ([117]). Moreover, infrared spectroscopy provides major information about cool astronomical regions in space, such as interstellar medium [118] and planetary nebulae [119]. It is found that $5p_{1/2} \rightarrow 4f_{5/2}$ of Kr^{7+} and $5p_{1/2} \rightarrow 5p_{3/2}$ of Xe^{7+} emit orange and green lights, respectively, which can be used in laser spectroscopy [120–124].

It is found from Table 5 that the $M1$ transition probability is stronger among fine-structure levels than the $E2$ transition. Table 4 reveals that the maximum $M1$ transition probability, A^{M1}_{RCC}, occurs for the transition $3p_{1/2} \rightarrow 3p_{3/2}$ of Ar^{7+}, $4p_{1/2} \rightarrow 4p_{3/2}$ of Kr^{7+}, $4f_{7/2} \rightarrow 5f_{7/2}$ of Xe^{7+} and $6p_{1/2} \rightarrow 6p_{3/2}$ of Rn^{7+}, and they have values of 0.17949, 8.4000, 158.33 and 1137.7, respectively. Moreover, our estimations of $M1$ transition probability for the $4f_{5/2} \rightarrow 4f_{7/2}$ transition of Xe^{7+} has excellent agreement with the calculations using the multi-configuration Dirac–Hartree–Fock method [125,126]. Table 6 presents the lifetime of the low-lying states of this series. We compare our results with other experimental and theoretical estimations wherever available and find good agreement with the recent endeavors. We provide lifetimes of many excited states calculated for the first time in the literature to our knowledge.

The comparisons of our computed results with the other estimations obtained from correlation exhaustive ab initio theoretical computations or precise experiments are one of the measures of accuracy of our calculations. Further, the differences between the calculated matrix elements in the length and velocity gauge forms are characteristic of the preciseness of our calculations. A recent piece of literature [95] also claims that the difference in length gauge and velocity gauge is a measure of accuracy. Another factor of accuracy in ab initio calculations arises from the DF wavefunctions used for correlation calculations. In addition, we should consider the uncertainty that arises from the other correlation terms (which we did not consider in this article) and the quantum electrodynamics effect, which is at most 2% in total. Taking all these into account, the maximum calculated uncertainties for Ar^{7+}, Kr^{7+}, Xe^{7+}, and Rn^{7+} are about 5.6%, 5.37%, 5% and 5.01%, respectively.

To understand the critical effect of the plasma atmosphere on the ionization potential of the ions, we highlight the IPD values in bold fonts in Table 1 for different values of screening length, μ. These IPD values reflect critical electron or plasma density at

a particular temperature for the ionic system when a few of the bound ionic states are elevated to continuum states.

Table 1 also reveals that the fine structure splittings (FSS) are suppressed as the screening strength increases from μ = 0 to 1.0. For example, the energy differences between $4p_{3/2}$ and $4p_{1/2}$ of Kr^{7+} are evaluated as 9774 a.u, 9732 a.u, 9608 a.u., and 9407 a.u. for μ = 0, 0.025, 0.05, and 0.075 a.u., respectively. This phenomenon is consistent with earlier calculations for sodium D line [127] and hydrogen-like atoms [128]. The suppression of the transition rate among the fine-structure levels is mainly arising from the energy quench.

From Figure 3, we pictorially estimate the critical values of plasma screening strength (μ_c) where the ionization potential becomes zero for a particular atomic state. We also tabulate these values in Table 7. The critical screening strength is essential in photo-ionization cross-section, which increases with increasing μ until $\mu = \mu_c$. This increment is obvious due to the decrease in bound state energy leading to the increase in radial expansion of the bound state wavefunction [128]. This phase shift of bound state to continuum state is induced by the plasma atmosphere, and the ionization threshold decreases with the Debye screening length (μ^{-1}). In terms of the photo-ionization cross-section [129], the plasma decreases the threshold cross-section, and the discrete bound wavefunctions become diffused. Therefore, critical screening strength plays an important role in atomic structure. However, we have not found any spectroscopic data in the literature for these ions in plasma medium to compare with our results.

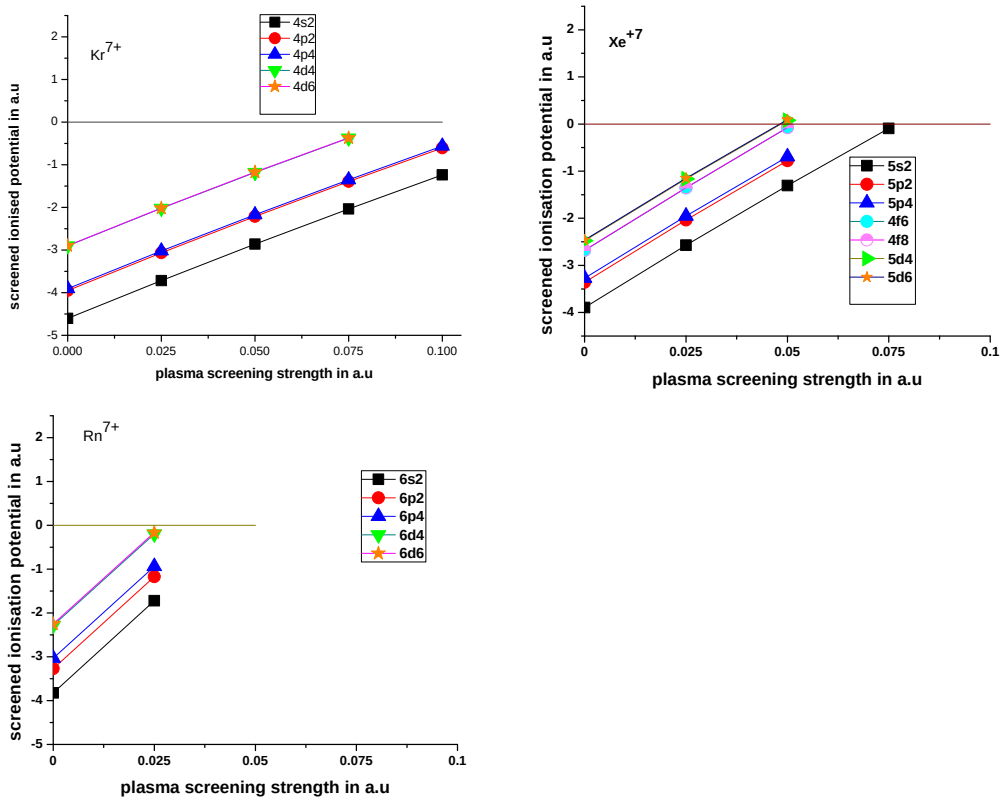

Figure 3. Determination of the value of critical plasma screening strength.

Table 4. Transition rate (in s^{-1}) of E2 (A^{E2}_{RCC}) in plasma screened and unscreened medium. Here, we have used our RCC matrix element (in a.u) and RCC wavelength (in Å). Note that the notation $P(Q)$ in the case of transition rates means $P \times 10^{Q}$.

Transitions	$\mu = 0$	$\mu = 0.025$	$\mu = 0.050$	$\mu = 0.075$	$\mu = 0.1$
Ar^{7+}					
3p4 → 4f6	1.4501 (+06)	1.4349 (+06)	1.3927 (+06)	1.3250 (+06)	1.2333 (+06)
3p4 → 4f8	6.5288 (+06)	6.4605 (+06)	6.2705 (+06)	5.9658 (+06)	5.5526 (+06)
3s2→ 3d4	2.1840 (+05)	2.2032 (+05)	2.2179 (+05)	2.2417 (+05)	2.2742 (+05)
3s2⟶ 3d6	2.1919 (+05)	2.2126 (+05)	2.2256 (+05)	2.2494 (+05)	2.2819 (+05)
3d4 → 5g8	2.7225 (+06)	2.6258 (+06)	2.3685 (+06)	1.9874 (+06)	
3d6 → 5g8	3.0252 (+05)	2.9179 (+05)	2.6352 (+05)	2.2077 (+05)	
3d6 → 5g10	3.0267 (+06)	2.9190 (+06)	2.6362 (+06)	2.2085 (+06)	
Kr^{7+}					
4s2⟶ 4d4	8.9514 (+05)	8.7868 (+05)	8.6208 (+05)	8.3473 (+05)	
4s2⟶ 4d6	9.1180 (+05)	8.9640 (+05)	8.7912 (+05)	8.5066 (+05)	
5p2 → 4f6	7.0537 (−01)	8.9779 (−01)	3.0592 (00)		
5p4 → 4f8	2.3536 (−01)	2.9840 (−01)	1.4702 (00)		
5d6 → 5g8	2.7840 (+03)	2.6100 (+03)			
5d6 → 5g10	2.9352 (+04)	2.6114 (+04)			
Xe^{7+}					
5s2→ 5d4	6.6714 (+05)	6.7116 (+05)			
5s2→ 5d6	6.9674 (+05)	7.0069 (+05)			
5p2 → 5p4	6.0045 (−01)	6.1555 (−01)	5.6058 (−01)		
5p2 → 4f6	8.5467 (+03)	2.7288 (+04)	3.3098 (+04)		
5p4 → 4f6	1.2882 (+03)	2.0657 (+03)	2.6049 (+03)		
5p4 → 4f8	5.9866 (+03)	1.2836 (+04)	1.6523 (+04)		
5p2→ 5f6	1.6471 (+06)	1.5379 (+06)			
5p4→ 5f6	4.3300 (+05)	4.0395 (+05)			
5p4→ 5f8	1.9479 (+06)	1.8169 (+06)			
4f6 → 5f6	5.9296 (+04)	5.4103 (+04)			
4f6 → 5f8	7.4168 (+03)	6.7680 (+03)			
4f8 → 5f6	9.9224 (+03)	9.0350 (+03)			
4f8 → 5f8	6.2129 (+04)	5.6576 (+04)			
5d4→ 6s2	5.3813 (+03)				
5d4 → 5g8	1.1670 (+06)				
5d6 → 5g8	1.2597 (+05)				
5d6→ 5g10	1.2601 (+06)				
5d6→ 6s2	7.0259 (+03)				
Rn^{7+}					
6s2 → 6d4	1.0243 (+06)	9.8377 (+05)			
6s2 → 6d6	1.0371 (+06)	9.9749 (+05)			
6p2 → 5f6	5.0885 (+04)	5.4520 (+04)			
6p4 → 5f6	3.2019 (+03)	3.5290 (+03)			
6p4 → 5f8	1.5773 (+04)	1.7127 (+04)			
6d4 → 5g8	6.3782 (+05)				
6d6 → 5g8	6.2707 (+04)				
6d6 → 5g10	6.2238 (+05)				
6p2 → 6p4	1.2855 (+02)	1.2763 (+02)			
7p2 → 7p4	1.5299 (+01)				
6p4 → 7p4	2.3245 (+05)				
5f6 → 7p2	1.4611 (+04)				
5f6 → 7p4	3.0317 (+03)				
5f8 → 7p4	1.7756 (+04)				

Table 5. Magnetic dipole transition rate (in s^{-1}) in plasma screened and unscreened medium. Note: the notation $P(Q)$ in the case of transition rates means $P \times 10^{Q}$. For $4f_{5/2} \rightarrow 4f_{7/2}$ (Xe^{7+}), transition rates 1.9227 (−03) and 1.9277 (−03) are available in the literature (a) using the multiconfiguration Dirac–Fock method without and with Breit interaction plus the quantum electrodynamics effect, respectively.

Transitions	$\mu = 0$	$\mu = 0.025$	$\mu = 0.050$	$\mu = 0.075$	$\mu = 0.1$
Ar^{7+}					
3p2 → 3p4	1.7951 (−01)	1.9857 (−01)	1.9603 (−01)	1.9165 (−01)	1.8570 (−01)
3p4 → 4f6	3.7845 (−02)	3.7248 (−02)	3.5575 (−02)	3.2958 (−02)	2.9561 (−02)
3d6 → 5g8	1.0634 (−02)	1.0124 (−02)	8.8719 (−03)	7.0637 (−03)	
Kr^{7+}					
4s2→ 4d4	9.0675 (−03)	7.2173 (−03)	8.2040 (−03)	6.7390 (−03)	
4p2 → 4p4	8.4015 (00)	8.2789 (00)	7.9664 (00)	7.4776 (00)	6.8397 (00)
4d4 → 4d6	2.5436 (−02)	3.2234 (−02)	3.0177 (−02)	2.7000 (−02)	
5p2 → 5p4	4.7841 (−01)	5.3517 (−01)	4.6911 (−01)		
5d4 → 5d6	1.7080 (−03)	1.0904 (−03)	2.2682 (−03)		
Xe^{7+}					
5p2 → 5p4	5.7437 (+01)	5.7875 (+01)	5.3500 (+01)		
5p4 → 5f6	6.3588 (−03)	5.7557 (−03)			
4f6 → 5f6	5.0459 (+01)	4.9605 (+01)			
4f6 → 5f8	4.9212 (−01)	5.3389 (−01)			
4f8 → 5f6	1.1142 (+01)	1.0620 (+01)			
4f8 → 5f8	1.5833 (+02)	1.5517 (+02)			
5d4 → 5d6	2.7070 (−01)	2.6538 (−01)	2.2900 (−01)		

Table 5. *Cont.*

Transitions	$\mu = 0$	$\mu = 0.025$	$\mu = 0.050$	$\mu = 0.075$	$\mu = 0.1$
Rn^{7+}					
6p2 → 6p4	1.2442 (+03)	1.2212 (+03)			
6d4 → 6d6	4.5873 (00)	4.1847 (00)			
5f6 → 5f8	6.6129 (−02)	3.4422 (−02)			
6s2 → 7s2	1.0113 (00)				
7p2 → 7p4	8.1938 (+01)				
6p2 → 7p2	7.2065 (−02)				
6p4 → 7p4	2.4557 (00)				
5f6 → 7p4	2.4281 (−03)				

[125,126].

Table 6. Lifetimes in ns of few low-lying states.

Level	Present Work	Other Work (Experiment)	Other Work (Theory)
Ar^{7+}			
3p2	0.411	0.417 ± 0.010 [a], 0.423 ± 0.040 [b], 0.48 ± 0.05 [g], 0.49 ± 0.05 [h] 0.55 ± 0.03 [l], 0.53 ± 0.11 [m]	0.413 [c], 0.407 [d], 0.397 [e], 0.409 [f] 0.389 [i], 0.408 [j], 0.4121 [k]
3p4	0.387	0.389 ± 0.010 [a], 0.421 ± 0.030 [b], 0.428 ± 0.027 [g], 0.48 ± 0.06 [h] 0.54 ± 0.0.02 [l], 0.527 ± 0.018 [m]	0.389 [c], 0.382 [d], 0.373 [e], 0.386 [f] 0.366 [i], 0.388 [j], 0.3872 [k]
3d4	0.132	0.170 ± 0.0.010 [a], 0.130 ± 0.005 [b], 0.158 ± 0.008 [g],	0.127 [e], 0.134 [f], 0.133 [j], 0.1318 [k]
3d6	0.137	0.166 ± 0.008 [a], 0.131 ± 0.005 [b], 0.160 ± 0.008 [g]	0.131 [e], 0.138[f,j], 0.1361 [k]
4f6	0.003		
4f8	0.002		
Kr^{7+}			
4p2	0.293	0.41 ± 0.04 [n], 0.291 ± 0.012 [o] 0.290 ± 0.015 [g], 0.401 ± 0.018 [l]	0.282 [p], 0.29653 [q]
4p4	0.235	0.33 ± 0.03 [n], 0.243 ± 0.01 [o] 0.218 ± 0.033 [g], 0.331 ± 0.011 [l]	0.230 [p], 0.24176 [q]
4d4	0.048		0.05019 [q]
4d6	0.052	0.048 ± 0.004 [o]	0.05388 [q]
4f6	0.055		
4f8	0.055		
Xe^{7+}			
5p2	0.45	0.52 (3) [r], 0.50 ± 0.05 [s], 0.380 ± 0.040 [g]	0.37 [t], 0.47 [u], 0.48 [v], 0.53 [w]
5p4	0.29	0.35 (2) [r], 0.33 ± 0.03 [s], 0.272 ± 0.037 [g]	0.23 [t], 0.30 [u], 0.31 [v], 0.33 [w]
5d4	0.08	0.10 (2) [r]	0.07 [t], 0.07 [v], 0.06 [w]
5d6	0.08	0.14 (2) [r]	0.14 [t], 0.08 [v], 0.07 [w]
Rn^{7+}			
6p2	0.429		
6p4	0.144		
6d4	0.056		
6d6	0.082		

a ⟹ Beam-foil technique [97]; *b* ⟹ [130]; *c* ⟹ third-order many-body perturbation theory [131]; *d* ⟹ R-matrix theory [98]; *e* ⟹ single Configuration interaction Hartree–Fock method using a pseudo potential [99]; *f* ⟹ relastic model potential [103]; *g* ⟹ Arbitrarily Normalized Decay curve method for cascade-correction in beam-foil [107]; *h* ⟹ beam-foil technique in the vacuum u.v [132]; *i* ⟹ Multiconfiguration Dirac–Fock method [104]; *j* ⟹ charge expansion technique [133]; *k* ⟹ multiconfiguration Dirac–Hartree–Fock theory including core polarization [31]; *l* ⟹ beam-foil [50]; *m* ⟹ beam-foil [134]; *n* ⟹ beam-foil [49]; *o* ⟹ foil excitation [106]; *p* ⟹ Coulomb approximation [111]; *q* ⟹ Hartree–Slater method [23]; *r* ⟹ beam-foil spectroscopy [53]; *s* ⟹ relativistic Hartree–Fock method [135]; *t* ⟹ relativistic perturbation theory with a zero approximation model potential [57]; *u* ⟹ relativistic many-dody perturbation theory(RMBPT(3)) [55]; *v* ⟹ relativistic HFR+CP [53]; *w* ⟹ relativistic MCDF [53].

Table 7. Critical values of plasma screening strength (μ_c) in a.u. for the following ions.

Kr^{7+}		Xe^{7+}		Rn^{7+}	
State	μ_c	**State**	μ_c	**State**	μ_c
4d4	0.087152	5s2	0.076987	5s2	0.046401
4d6	0.086956	5p2	0.066149	6p2	0.039652
		5p4	0.064474	6p4	0.036763
		4f6	0.051526	6d4	0.027521
		4f8	0.051486	6d6	0.027100
		5d4	0.048395		
		5d6	0.048139		

4. Conclusions

The continuous progress in astrophysical and astronomical observations demands accurate theoretical transition data in a realistic environment. In many cases, the experiment is difficult to extract the data used to estimate the abundance of the ions in the stellar chemical composition. Here, the highly correlated relativistic coupled-cluster theory is applied to precisely determine the excitation energies of a few low-lying states of astrophysically relevance such as Ar^{7+}, Kr^{7+} and Xe^{7+}, and Rn^{7+}. Furthermore, we calculate various properties of allowed and forbidden transitions, such as transition probabilities, oscillator strengths, and lifetimes, and compare them with previously reported data in the literature. We found an overall good agreement between our results with the other theoretical and experimental results. Moreover, the concurrence between the length and velocity gauge allowed transition amplitudes signifies the exact calculations of our correlated wavefunctions. We found that most of the transitions shown here fall in the ultraviolet region of the electromagnetic spectrum, useful for astrophysical plasma research and telescope-based astronomy. A few transitions, such as $4d_{3/2} - 4f_{5/2}$, $4d_{5/2} - 4f_{5/2}$ and $4d_{5/2} - 4f_{7/2}$ of Ar^{7+}, $5p_{1/2} - 4f_{5/2}$ of Kr^{7+} and $5p_{1/2} - 5p_{3/2}$ of Xe^{7+} emit the visible light, which can have application in laser spectroscopy. Our presented transition line parameters of Rn^{7+} may help the astronomer identify the ion's unknown lines. To the best of our knowledge, some of the oscillator strengths of allowed transitions and most of the transition rates of the forbidden transitions are reported here for the first time in the literature.

The main focus of this paper is to evaluate the above spectroscopic properties under a realistic astronomical atmosphere. We showed that the variation of our results for different values of Debye screening lengths and ionization potential depression values for each atomic state are useful for atomic structure characterization.

Author Contributions: S.B. and S.M. have visualize and conceptualize the problem, S.B. has augmented the code for plasma environment, did former analysis, data curation. All the authors worked on the manuscript. S.M. has supervised the total work. All authors have read and agreed to the published version of the manuscript.

Funding: This research received no external funding

Data Availability Statement: Not applicable.

Conflicts of Interest: The authors declare no conflict of interest.

References

1. Barlow, M.J.; Swinyard, B.M.; Owen, P.J.; Cernicharo, J.; Gomez, H.L.; Ivison, R.J.; Krause, O.; Lim, T.L.; Matsuura, M.; Miller, S.; Olofsson, G.; Polehampton, E.T. Detection of a Noble Gas Molecular Ion $^{36}ArH^+$. *Science* **2013**, 342, 1343–1345. https://doi.org/10.1126/science.1243582.
2. Güsten, R.; Wiesemeyer, H.; Neufeld, D.; Menten, K.; Graf, U.; Jacobs, K.; Klein, B.; Ricken, O.; Risacher, C.; Stutzki, J. Astrophysical detection of the helium hydride ion HeH^+. *Nature* **2019**, *568*, 357–359. https://doi.org/10.1038/s41586-019-1090-x.
3. Benna, M.; Mahaffy, P.R.; Halekas, J.S.; Elphic, R.C.; Delory, G.T. Variability of helium, neon, and Argom in the lunar exosphere as observed by the LADEE NMS instrument. *Geophys. Res. Lett.* **2015** *42*, 3723. https://doi.org/10.1002/2015GL064120.
4. Müller, H.S.P.; Muller, S.; Schilke, P.; Bergin, E.A.; Black, J.H.; Gerin, M.; Lis, D.C.; Neufeld, D.A.; Suri, S. Detection of extragalatic argonium ArH^+, towards PKS 1830-211. 2015, *Astron. Astrophys.* **2015**, *582*, L4. https://doi.org/10.1051/0004-6361/201527254.
5. Schilke, P.; Neufeld, D.; Mueller, H.; Comito, C.; Bergin, E.; Lis, D.; Gerin, M.; Black, J.H.; Wolfire, M.; Indriolo, N.; et al. Ubiquitous argonium (ArH^+) in the diffuse interstellar medium: A molecular tracer of almost purely atomic gas. *Astron. Astrophys.* **2014**, *566*, A29. https://doi.org/10.1051/0004-6361/201423727.
6. Taresch, G.; Kudritzki, R.P.; Hurwitz, M.; Bowyer, S.; Pauldrach, A.W.A.; Puls, J.; Butler, K.; Lennon, D.J.; Haser, S.M. Quantitative analysis of the FUV, UV and optical spectrum of the O3 star HD 93129A. *Astron. Astrophys.* **1997**, *321*, 531–548.
7. Pérez-Montero, E.; Hägele, G.F.; Contini, T.; Díaz, Á.I. Neon and Argon optical emission lines in ionized gaseous nebulea: Implications and aplications. *Mon. Not. R. Astron. Soc.* **2007**, *381*, 125–135. https://doi.org/10.1111/j.1365-2966.2007.12213.x.
8. Panigrahy, S.N.; Dougherty, R.W.; Das, T.P.; Andriessen, J. Theory of hyperfine interactions in lithiumlike systems. *Phys. Rev. A* **1989**, *40*, 1765. https://doi.org/10.1103/PhysRevA.40.1765.
9. Owusu, A.; Yuan, X.; Panigrahy, S.N.; Doughetry, R.W.; Das, T.P. Andriessen, J. Theory of hyperfine interactions in potassium and Sc^{2+} Sion: Trends in system isoelectronic with Potassium. *Phys. Rev. A* **1977**, *55*, 2644. https://doi.org/10.1103/PhysRevA.55.2644.

10. Xiao, L.W.; Kai-Zhi, Y.; Bing-Cong, G.; Meng, Z. Calculation on the hyperfine constants of the ground states for Lithium-like system. *Chin. Phys.* **2007**, 16, 2389. https://doi.org/10.1088/1009-1963/16/8/039.
11. Roy, S.N.; Rodgers, J.E.; Das, T.P. Hyperfine interactions in stripped atoms isoelectronic with alkali atoms. *Phys. Rev. A* **1976**, *13*, 1983. https://doi.org/10.1103/PhysRevA.13.1983.
12. Dutta, N.N.; Majumder, S. Electron-correlation trends in the hyperfine A and B constant of Na isoelectronic sequence. *Phys. Rev. A* **2013**, *88*, 062507. https://doi.org/10.1103/PhysRevA.88.062507.
13. Herrnstein, J.R.; Moran, J.M.; Greenhill, L.J.; Dimond, P.J.; Inoue, M.; Nakai, N.; Miyoshi, M.; Henkel, C.; Riess, A. A geometric distance to the Galaxy NGC4258 from orbital motions in a nuclear gas disc. *Nature* **1999**, *400*, 539–541. https://doi.org/10.1038/22972.
14. Dimitrijevć, M.S. Stark broadening in astrophysics. *Astron. Astrophys. Trans.* **2003**, *22*, 389–412. https://doi.org/10.1080/1055679031000108167.
15. Eldén, B. Die deutung der Emissionslinien im spektrum der sonnenkorona. *Z. Astrophys.* **1942**, *22*, 30.
16. Eidelsberg, M.; Crifo-Magnant, F.; Zeippen, C.J. Forbidden lines in hot astronomical sources. *Astron. Astrophys. Suppl. Ser.* **1981**, *43*, 455–471.
17. Mcwhirter, R.W.P.; Summers, H.P. Atomic radiation from low density plasma. *Appl. At. Collission Phys.* **1983**, *2*, 51.
18. Eldén, B. Forbidden lines in hot plasma. *Phys. Scr.* **1984**, *26*, 71.
19. Sterling, N.C.; Dinerstein, L.H.; Charles, B.W. Discovery of enhanced Germanium abundances in planetary nebulae with the *far ultraviolet spectroscopic explorer*. *Astrophys. J.* **2002**, *578*, L55.
20. O'Toole, S.J. beyond the iron group: Heavy metals in hot subdwarfs. *Astron. Atrophys.* **2004**, *423*, L25–L28. https://doi.org/10.1051/0004-6361:200400027.
21. Chayer, P.; Vennes, S.; Dupuis, J.; Kruk, J.W. Abundance of elements beyond the Iron group in cool DO white Dwarfs. *Astrophys. J.* **2005**, *630*, L169. https://doi.org/10.1086/491699.
22. Vennes, S.; Chayer, P.; Dupuis, J. Discovery of photospheric Germanium in Hot DA White Dwarfs. *Astrophys. J.* **2005**, *622*, L121. https://doi.org/10.1086/429667.
23. Curtis, L.J.; Theodosiou, C.E. Comprehensive calculations of 4p and 4d lifetimes for the Cu sequence. *Phys. Rev. A* **1989**, *39*, 605. https://doi.org/10.1103/PhysRevA.39.605.
24. Dimitrijevć, M.S.; Simić, Z.; Kovačević, A.; Valjarević, A.; Sahal-Bréchot, S. Stark broadening of Xe VIII spectral lines. *Mon. Not. R. Astron. Soc.* **2015**, *454*, 1736–1741. https://doi.org/10.1093/mnras/stv1970.
25. Beer, H.; Käppeler, F.; Reffo, G.; Venturini, G. Neutron capture cross-sections of stable xenon isotopes and their application in stellar nucleosynthesis. *Astrophys. Space Sci.* **1983**, *97*, 95. https://doi.org/10.1007/BF00684613.
26. Clayton, D.D.; Ward, R.A. S process studies: Xenon and krypton isotopic abundances. *Astrophys. J.* **1978**, *224*, 1000. https://ui.adsabs.harvard.edu/link_gateway/1978ApJ...224.1000C/doi:10.1086/156449.
27. Berry, H.G.; Hallin, R.; Sjödin, R.; Gaillard, M. Beam -foil observations of Na 1 doubly-excited states. *Phys. Lett.* **1974**, *50A*, 191. https://doi.org/10.1016/0375-9601(74)90784-1.
28. Striganov, A.R.; Odintsova, G.A. *Tables of Spectral Lines of Atom and Ions*; Energy: Moscow, Russia, 1982.
29. Jupén, C.; Engström, L.; Hutton, R.; Reistad, N.; Westrlind, M. Analysis of core-excited n = 3 configurations in S VI, Cl VII, Ar VIII, and Ti XII. *Phys. Scr.* **1990**, *42*, 44. https://doi.org/10.1088/0031-8949/42/1/007.
30. Biémont, E.; Frémat, Y.; Quinet, P. Ionization potentials of atoms and ions from Lithium to Tin (z = 50). *At. Nucl. Data Tables* **1999**, *71*, 117. https://doi.org/10.1006/adnd.1998.0803.
31. Fischer, C.F.; Tachiev, G.; Irimia, A. Relativistic energy levels, lifetimes, and transition probabilities for the sodium-like to argon-like sequences. *At. Nucl. Data Tables* **2006**, *92*, 607. https://doi.org/10.1016/j.adt.2006.03.001.
32. Saloman, E.B. Energy levels and observed spectral lines of ionized Argon, Ar II through Ar XVIII. *J. Phys. Chem. Ref. Data* **2010**, *39*, 033101. https://doi.org/10.1063/1.3337661.
33. Cardelli, J.A.; Mayer, D.M. The Abundance of Interstellar krypton. *Astrophys. J.* **1997**, *477*, L57. https://doi.org/10.1086/310513.
34. Cardelli, J.A.; Sarage, B.D.; Ebbets, D.C. Interstellar Gas phase Abundance Carbon, Oxygen, Nitrogen, Copper, Gallium, Germanium, and Krypton toward zeta ophiuchi. *Astrophys. J. Lett.* **1991**, *383*, L23. https://ui.adsabs.harvard.edu/link_gateway/1991ApJ...383L..23C/doi:10.1086/186232.
35. Cartledge, S.I.B.; Meyer, D.M.; Lauroesch, J.T. The Homogeneity of Interstellar Krypton in the Galactic Disk. *Astrophys. J.* **2003**, *597*, 408–413. https://ui.adsabs.harvard.edu/link_gateway/2003ApJ...597..408C/doi:10.1086/378323.
36. Dinerstein, H.L. Neutron-Capture Elements in Planetary Nebulae: Identification of two near-Infrared Emission Lines as [Kr III]. *Astrophy. J.* **2001**, *550*, L223–L226. https://doi.org/10.1086/319645.
37. Cheng, K.-T.; Kim, Y.-K. Energy levels, wavelengths, and transition probabilities of Cu-like ions. *At. Data Nucl. Data Tables* **1978**, *22*, 547–563. https://doi.org/10.1016/0092-640X(78)90023-2.
38. Reader, J.; Acquista, N.; Kaufman, V. Spectrum and energy levels of seven-times-ionized Krypton (Kr VIII) and resonance lines of eight-times-ionized Krypton (Kr VIII). *J. Opt. Soc. Am. B* **1991**, *8*, 538–547. https://doi.org/10.1364/JOSAB.8.000538.
39. Boduch, P.; Chantepie, M.; Hennecart, D.; Husson, X.; Lecler, D.; Druetta, M.; Wilson, M. Spectroscopic analysis of visible and near UV light emitted in 120-kev Kr^{8+}-He and Kr^{8+}-H_2 collisions. *Phys. Scr.* **1992**, *46*, 337. https://doi.org/10.1088/0031-8949/46/4/004.

40. Johnson, W.R.; Blundell, S.A.; Sapirstein, J. Many-body perturbation-theory calculations of energy levels along the copper isoelectronic sequence. *Phys. Rev. A* **1990**, *42*, 1087. https://doi.org/10.1103/PhysRevA.42.1087.
41. Vilkas, M.J.; Ishikawa, Y.; Hirao, K. Ionization energies and fine structure splitting of highly correlated systems: Zn, zinc-like ions and Copper-like ions. *Chem. Phys. Lett.* **2000**, *321*, 243–252. https://doi.org/10.1016/S0009-2614(00)00361-4.
42. Hinnov, E. Highly ionized atoms in tokamak discharges. *Phys. Rev. A* **1976**, *14*, 1533. https://doi.org/10.1103/PhysRevA.14.1533.
43. Alexander, E.; Even-Zohar, M.; Fraenkel, B.S.; Goldsmith, S. Classification of transitions in the EUV spectra of Y ix-xiii, Zn x-xiv, Nb xi-xv and Mo xii-xvi, *J. Opt. Soc. Am.* **1971** , *61*, 508. https://opg.optica.org/josa/abstract.cfm?URI=josa-61-4-508.
44. Reader, J.; Acquista, N. 4s-4p resonance transitions in highly charged Cu- and Zn-like ions. *Phys. Rev. Lett.* **1977**, *39*, 184. https://doi.org/10.1103/PhysRevLett.39.184.
45. Curtis, L.J.; Lindgård, A.; Eldén, B.; Martinson, I.; Nielsen, S.E. Energy levels and transition probabilities in Mo XIV. *Phys. Scr.* **1977** *16*, 72. https://doi.org/10.1088/0031-8949/16/1-2/012.
46. Joshi, Y.N.; van Kleef, Th, A.M. The sixth spectrum of selenium: Se VI. *Physica B+C* **1978**, *94*, 270–274. https://doi.org/10.1016/0378-4363(78)90152-3.
47. Reader, J.; Luther, G.; Acquista, N. Spectrum and energy levels of thirteen-times ionized Molybdenum Mo XIV. *J. Opt. Soc. Am.* **1979**, *69*, 144–149. https://doi.org/10.1364/JOSA.69.000144.
48. Mansfield, M.W.D.; Peacock, N.J.; Smith, C.C.; Hobby, M.G.; Cowan, R.D. The XUV spectra of highly ionized Molybdenum. *J. Phys. B Atom. Mol. Phys.* **1978**, *11*, 1521–1544. https://doi.org/10.1088/0022-3700/11/9/008.
49. Druetta, M.; Buchet, J.P. Beam-foil study of krypton between 400 and 800 Å. *J. Opt. Soc. Am.* **1976**, *66*, 433. https://doi.org/10.1364/JOSA.66.000433.
50. Irwin, D.J.G.; Karnahan, J.A.; Pinnington, E.H.; Livingston, A.E. Beam-foil mean-life measurements in krypton. *J. Opt. Soc. Am.* **1976**, *66*, 1396–1400. https://doi.org/10.1364/JOSA.66.001396.
51. Knystautas, E.J.; Drouin, R. Oscillator strength of resonance lines in Br(VI), (VII) and Kr(VII), (VIII). *J. Quant. Spectrosc. Radiat. Transfer.* **1977**, *17*, 551–553. https://doi.org/10.1016/0022-4073(77)90103-0.
52. Werner, K.; Rauch, T.; Ringat, E.; Kruk, J.W. First detection of Krypton and Xenon in a white dwarf. *Astrophys. J. Lett.* **2012**, *753*, L7. https://doi.org/10.1088/2041-8205/753/1/L7.
53. Biémont, E.; Clar, M.; Fivet, V.; Garnir, H.-P.; Palmeri, P.; Quinet, P.; Rostohar, D. Lifetime and transition probability determination in xenon ions. *Eur. Phys. J. D* **2007**, *44*, 23–33. https://doi.org/10.1140/epjd/e2007-00161-2.
54. Migdalek, J.; Garmulewicz, M. The relativistic ab initio model potential versus Dirac–Fock oscillator strengths for silver and gold isoelectronic sequences. *J. Phys. B At. Mol. Opt. Phys.* **2000**, *33*, 1735. https://doi.org/10.1088/0953-4075/33/9/305.
55. Safronova, U.I.; Savukov, I.M.; Safronova, M.S.; Johnson, W.R. Third-order relativistic many-body calculations of energies and lifetimes of levels along the silver isoelectronic sequence. *Phys. Rev. A* **2003**, *68*, 062505. https://doi.org/10.1103/PhysRevA.68.062505.
56. Glowacki, L.; Migdałek, J. Relativistic configuration-interaction Oscillator strength for lowest E1 transitions in silver and gold isoelectronic sequences. *Phys. Rev. A* **2009**, *80*, 042505. https://doi.org/10.1103/PhysRevA.80.042505.
57. Ivanova, E.P. Transitions probabilities for 5s-5p, 5p-5d, 4f-5d, and 5d-5f transitions in Ag-like ions with Z = 50–86. *At. Data Nucl. Data Tables* **2011** , *97*, 1–22. https://doi.org/10.1016/j.adt.2010.06.005.
58. Otsuka, M.; Tajitsu, A. Chemical abundances in the Carbon-rich and Xenon-rich halo planetary nebula H4-1. *Astrophys. J.* **2013**, *778*, 146. https://doi.org/10.1088/0004-637X/778/2/146.
59. Bhowmik, A.; Dutta, N.N.; Roy, S. Precise calculations of Astrophysically Important Allowed and Forbidden Transitions of Xe VIII. *Astrophys. J.* **2017**, *836*, 125. https://doi.org/10.3847/1538-4357/836/1/125.
60. Pernpointner, M.; Zobel, J.P.; Kryzhevoi, N.V. Strong configuration interaction in the double ionization spectra of noble gases studied by the relativistic propagator method. *Phys. Rev. A* **2012**, *85*, 012505. https://doi.org/10.1103/PhysRevA.85.012505.
61. Eser, S.; Özdemir, L. Energies and lifetimes of levels for doubly ionized Xenon and Radon. *Phys. Pol. A* **2018**, *133*, 1324. https://doi.org/10.12693/APhysPolA.133.1324.
62. Pequignot, D.; Baluteau, J.-P. The identification of krypton, xenon and other elements of rows 4, 5, and 6 of the periodic table in the planetary nebula NGC 7027. *Astron. Astrophys.* **1994**, *283*, 593–625.
63. Migdalek, J. Core-polarisation corrected relativistic energy and radiative data for one- electron spectra of Bi v through U XIV. *Can. J. Phys.* **2018**, *96*, 610. https://doi.org/10.1139/cjp-2017-0641.
64. Lindgren I.; Mukherjee, D. On the connectivity criteria in the open shell coupled-cluster theory for general model spaces. *Phys. Rep.* **1987**, *151*, 93–127. https://doi.org/10.1016/0370-1573(87)90073-1.
65. Bishope, R.F. An overview of coupled cluster theory and it's applications in physics. *Theor. Chim. Acta* **1991**, *80*, 95–148. https://doi.org/10.1007/BF01119617.
66. Roy, S.; Majumder, S. Ab initio estimations of the isotope shift for the first three elements of the K isoelectronic sequence. *Phys. Rev. A* **2015**, *92*, 012508. https://doi.org/10.1103/PhysRevA.92.012508.
67. Dutta, N.N.; Majumder, S. Accurate estimations of stellar and interstellar transition lines of triply ionized germanium. *Astrophys. J.* **2011**, *737*, 25. https://doi.org/10.1088/0004-637X/737/1/25[CrosssRef]
68. Dutta, N.N.; Majumder, S. Ab initio studies of electron correlation and Gaunt interaction effects in the boron isoelectronic sequence using coupled cluster theory. *Phys. Rev. A* **2012**, *85*, 032512. https://doi.org/10.1103/PhysRevA.85.032512.

69. Dutta, N.N.; Majumder, S. *Ab initio* calculations of spectroscopic properties of Cr^{5+} using coupled cluster-theory. *Indian J. Phy.* **2016**, *90*, 373. https://doi.org/10.1007/s12648-015-0754-0.
70. Bhowmik, A.; Roy, S.; Dutta, N.N.; Majumder, S. Study of Coupled-Cluster correlations on electromagnetic transitions and hyperfine structure constants of W VI. *J. Phys. B At. Mol. Opt. Phys.* **2017**, *50*, 125005. https://doi.org/.1088/1361-6455/aa6ccf.
71. Bhowmik, A.; Dutta, N.N.; Majumder, S. Magic wavelengths for trapping with focused Laguerre-Gaussian beams. *Phy. Rev. A* **2018**, *97*, 022511. https://doi.org/10.1103/PhysRevA.97.022511.
72. Bhowmik, A.; Dutta, N.N.; Majumder, S. Vector polarizability of an atomic state induced by a linearly polarized vortex beam. External control of magic tune-out wavelengths and heteronuclear spin oscillations. *Phy. Rev. A* **2020**, *102*, 063116. https://doi.org/10.1103/PhysRevA.102.063116.
73. Bhowmik, A.; Dutta, N.N.; Das, S. Role of vector polarizability induced by a linearly polarized focused Lagueree-Gaussian light:application in optical trapping and ultracold spinor mixture. *Eur. Phys. J. D* **2022**, *76*, 139. https://doi.org/10.1140/epjd/s10053-022-00470-y.
74. Biswas, S.; Das, A.; Bhowmik, A.; Majumder, S. Accurate estimations of electromagnetic transitions of Sn IV for stellar and interstellar media. *Mon. Not. R. Astron. Soc.* **2018**, *477*, 5605. https://doi.org/10.1093/mnras/sty1015.
75. Das, A.; Bhowmik, A.; Dutta, N.N.; Majumder, S. Many-body calculations and hyperfine-interaction effect on dynamic polarizabilities at low-lying energy levels of $\mathbf{Y}^{2+}$. *Phys. Rev. A* **2020**, *102*, 012801. https://doi.org/10.1103/PhysRevA.102.012801.
76. Das, A.; Bhowmik, A.; Dutta, N.N.; Majumder, S. Two-Photon Polarizability of Ba^{+} ion: Control of Spin-Mixing Process in an Ultracold $^{137}Ba^{+}$. *Atoms* **2022**, *10*, 109. https://doi.org/10.3390/atoms10040109.
77. Sahoo, B.K.; Majumder, S.; Chaudhuri, R.K.; Das, B.P.; Mukherjee, D. Ab initio determination of the lifetime of the $6^2P_{3/2}$ state for $^{207}Pb^{+}$ by relativistic many-body theory, *J Phys. B* **2004**, *37*, 3409. https://doi.org/10.1088/0953-4075/37/17/002.
78. Bartlett, R.J. *Modern Electronic Structure Theory*; Yarkony, D.R., Ed.; World Scientific: Singapore, 1995; Volume II, p. 1047.
79. Mondal, P.K.; Dutta, N.N.; Majumder, S. Effect of screening on spectroscopic properties of Li-like ions in a plasma medium. *Phys. Rev. A* **2013**, *87*, 062502. https://doi.org/10.1103/PhysRevA.87.062502.
80. Stewart, J.C.; Pyatt, K.D., Jr. Lowering of ionization potential in plasmas. *Astrophys. J.* **1966**, *144*, 1203. https://ui.adsabs.harvard.edu/link_gateway/1966ApJ...144.1203S/doi:10.1086/148714.
81. Szabo, A.; Ostlund, N.S. *Modern Quantum Chemistry: Int roduction to Advanced Elec-tronic Structure Theory*; Courier Corporation: Dover, Mineola, 1996.
82. Dixit, G.; Sahoo, B.K.; Chaudhuri, R.K.; Majumder, S. Ab initio calculations of forbidden transition amplitudes and lifetimes of the low-lying states in V^{4+}. *Phy. Rev. A* **2007**, *76*, 059901. https://doi.org/10.1103/PhysRevA.76.042505.
83. Lindgren, I.; Morrison, J. *Atomic Many-Body Theory*; Springer: Berlin/Heidelberg, Germany, 1986; Volume 3. https://doi.org/10.1007/978-3-642-61640-2.
84. Savukov, I.M.; Johnson, W.R.; Safronova, U.I. Multipole(E1, M1, E2, M2) transition wavelength and rates between states with n $\leq$ 6 in He-like Carbon, Nitrogen, Oxygen, Neon, Silicon and Argon. *At. Data Nucl. Data Tables* **2003**, *85*, 83–167. https://doi.org/10.1016/S0092-640X(03)00056-1.
85. Shore, B.W.; Menzel, D.H. *Principles of ATOMIC SPECTRA*; John Wiley and Sons: New York, NY, USA, 1968.
86. Kelleher, D.E.; Podobedova, L.I. Atomic transition probabilities of Sodium and Magnetium. A critical compilation. *J. Phys. Chem. Ref. Data* **2008**, *37*, 267. https://doi.org/10.1063/1.2735328.
87. Ichimaru, S. Strongly coupled plasmas: High-density classical plasmas and degenerate electron liquids. *Rev. Mod. Phys.* **1982**, *54*, 1017. https://doi.org/10.1103/RevModPhys.54.1017.
88. Akhiezer, A.I.; Akhiezer, I.A.; Polovin, R.V.; Sitenko, A.G.; Stepano, K.N. *Plasma Electrodynamics. Volume 1. Linear Theory*; Pergamon Press: New York, NY, USA, 1975; 431p.
89. Parpia, F.A.; Fischer, C.F.; Grant, I.P. GRASP92 a package for large-scale relativistic atomic structure calculations. *Comput. Phys. Commun.* **2006**, *175*, 745.
90. Clementi, E. (Ed.) *Modern Techniques in Computational Chemistry: MOTECC-90*; Springer: Amsterdam, The Netherlands, 1990.
91. Huzinaga, S.; Klobukowski, M. Well-tempered gaussian bassis set for the calculation of matrix Hartree-fock wave function. *Chem. Phys. Letts.* **1993**, *212*, 260–264. https://doi.org/10.1016/0009-2614(93)89323-A.
92. Roy, S.; Dutta, N.N.; Majumder, S. Relativistic coupled-cluster calculations on hyperfine structures and electromagnetic transition amplitudes of In III. *Phys. Rev. A* **2014**, *89*, 042511. https://doi.org/10.1103/PhysRevA.89.042511.
93. Kramida, A.; Ralchenko, Y.; Reader, J.; NIST ASD Team. *NIST Atomic Spectra Database (Ver. 5.10)*; National Institude of Standards and Technology: Gaithersburg, MD, USA, 2022. Available online: http://physics.nist.gov/asd (accessed on 10 March 2023).
94. Dutta, N.N.; Roy, S.; Dixit, G.; Majumder, S. Ab initio calculations of transition amplitudes and hyperfine A and B constants of Ga III. *Phys. Rev. A* **2013**, *87*, 012501. https://doi.org/10.1103/PhysRevA.87.012501.
95. Jyoti, K.H.; Arora, B.; Sahoo, B.K. Radiative properties of Cu-isoelectronic As, Se, and Br ions for astrophysical applications. *Mon. Not. R. Astron. Soc.* **2022**, *511*, 1999–2007. https://doi.org/10.1093/mnras/stac163.
96. Cowan R.D. *The Theory of Atomic Structure and Spectra*; University of California Press: Berkeley, CA, USA, 1981.
97. Reistad, N.; Engström, L.; Berry, H.G. Oscillator strength measurements of resonance transitions in Sodium- and Magnesium-like Argon. *Phys. Scr.* **1986**, *34*, 158. https://doi.org/10.1088/0031-8949/34/2/012.
98. Verner, D.A.; Verner, E.M.; Ferl, G.J. Atomic data for permitted resonance lines of atoms and ions from H to Si and S, Ar, Ca, and Fe. *At. Data Nucl. Data Tables* **1996**, *64*, 180. https://doi.org/10.1006/adnd.1996.0018.

99. Féret, L.; Pascale, J. Study of the multi charged ion Ar^{6+} by a configuration interaction Hartee Fock method using a pseudopotential. *J. Phys. Rev. B At. Mol. Opt. Phys.* **1999**, 32, 4175. https://doi.org/10.1088/0953-4075/32/17/304.
100. Lagmago, K.G.; Nana Engo, S.G.; Kwato Njock, M.G.; Oumarou, B. Consistent description Klein-Gordon dipole matrix elements. *J. Phys. B At. Mol. Opt. Phys.* **1998**, *31*, 963. https://doi.org/10.1088/0953-4075/31/5/007.
101. Siegel, W.; Migdalek, J.; Kim, Y.K. Dirac–Fock oscillator strengths for E1 transition in the sodium isoelectronic sequence(Na I-Ca X). *At. Data Nucl. Data Tables* **1988**, *68*, 303–322. https://doi.org/10.1006/adnd.1997.0769.
102. Guet, C.; Blundell, S.A.; Johnson, W.R. Relativistic Many-body calculations of oscillator strength for sodium-like ions. *Phys. Lett. A* **1990**, *143*, 384. https://doi.org/10.1016/0375-9601(90)90377-Z.
103. Theodosiou, C.E.; Curtis, L.J. Accurate calculations of 3p and 3d lifetimes in the Na sequence. *Phys. Rev. A* **1988**, *38*, 4435. https://doi.org/10.1103/PhysRevA.38.4435.
104. Kim, Y.-K.; Cheng, K.-T. Transition probabilities for the resonance transitions of Na-like ions. *J. Opt. Soc. Am.* **1978**, *68*, 836. https://doi.org/10.1364/JOSA.68.000836.
105. Gruzdev, P.F.; Sherstyuk, A.I. Relativistic generalization of the effective orbital quantum number method. *Opt. Spectrosc.* **1979**, *46*, 353–355.
106. Livingston, A.E.; Curtis, L.J.; Schectman, R.M.; Berry, H.G. Energies and lifetimes of excited states in Copper like Kr VIII. *Phys. Rev. A* **1980**, *21*, 771. https://doi.org/10.1103/PhysRevA.21.771.
107. Pinnington, E.H.; Gosselin, R.N.; O'Neill, J.A.; Kernahan, J.A.; Donnely, K.E.; Brooks, R.L. Beam-foil lifetime measurements using ANDC analysis for the resonance doublet in A VIII, Kr VIII and Xe VIII. *Phys. Scr.* **1979**, *20*, 151. https://doi.org/10.1088/0031-8949/20/2/005.
108. Fischer, C.F. Oscillator strength of $^2S - ^2P$ transitions in the copper sequence. *J. Phys. B* **1977**, *10*, 1241. https://doi.org/10.1088/0022-3700/10/7/013.
109. Weiss, A.W. Hartree–Fock line strength for the Lithium, Sodium, and Copper isoelectronic sequences. *J. Quant. Spectrosc. Radiat. Transf.* **1977**, *18*, 481–490. https://doi.org/10.1016/0022-4073(77)90046-2.
110. Cowan, R.D. *Los Alamos Report No. LA-6679, MS, National Information Service*; Spring: London, UK, 1977.
111. Lindgård, A.; Curtis, L.J.; Matrinson, I.; Nielsen S.E. Semi-Empirical Oscillator Strengths for Cu I Isoelectronic sequence. *Phys. Scr.* **1980**, *21*, 47. https://doi.org/10.1088/0031-8949/21/1/008.
112. Migdalek, J.; Baylis, W.E. Influence of core polarization on oscillator strength along the Copper isoelectronic sequence. *J. Phys. B Atom. Mol. Phys.* **1979**, *12*, 1113. https://doi.org/10.1088/0022-3700/12/7/014.
113. Saloman, E.B. Energy levels and observed spectral lines of Xenon, Xe I through Xe LIV. *J. Phys. Chem. Ref. Data* **2004**, *33*, 765. https://doi.org/10.1063/1.1649348.
114. Morita, S.; Goto, M.; Katai, R.; Dong, C.; Sakaue, H.; Zhou, H. Observation of Magnetic dipole forbiden transition in LHD and its application to burning plasma diagnostics. *Plasma Sci. Technol.* **2010**, *12*, 341. https://doi.org/10.1088/1009-0630/12/3/19.
115. Fahy, K.; Sokell, E.; O'Sullivan, G.; Aguilar, A.; Pomeroy J.M.; Tan, J.N.; Gillaspy, J.D. Extreme-ultraviolet spectroscopy of highly charged xenon created using an electron-beam ions trap. *Phys. Rev. A* **2007**, *75*, 032520. https://doi.org/10.1103/PhysRevA.75.032520.
116. Morgan, C.A.; Serpa, F.G.; Takacs, E.; Meyer, E.S.; Gillaspy, J.D.; Sugar, J.; Roberts, J.R.; Brown, C.M.; Feldman, U. Observation of visible and uv magnetic dipole transition in highly charged Xenon and Barium. *Phys. Rev. Lett.* **1995**, *74*, 1716. https://doi.org/10.1103/PhysRevLett.74.1716.
117. Kessler, M.F.; Steinz, J.A.; Anderegg, M.E.; Clavel, J.; Drechsel, G.; Estaria, P.; Faelker, J.; Riedinger, J.R.; Robson, A.; Taylor, B.G.; Ximénez de Ferrán, S. The Infrared Space Observatory (ISO) Mission. *Astron. Astrophys.* **1996**, *315*, L27–L31.
118. Feuchtgruber, H.; Lutz, D.; Beintema, D.A.; Valentijn, E.A.; Bauer, O.H.; Boxhoorn, D.R.; De Graauw, T.; Haser, T.N.; Haerendel, G.; Heras, A.M. New wavelength determination of mid-infrared fine structure lines by *infrared space observatory* short wavelength spectrometer. *Astrophys. J.* **1997**, *487*, 962. https://doi.org/10.1086/304649.
119. Liu, X.-W.; Barlow, M.J.; Cohen, M.; Danziger, I.J.; Luo, S.-G.; Baluteau, J.P.; Cox, P.; Emery, R.J.; Lim, T.; Péquignot, D. *ISO LWS* observations of planetary nebula fine-structure lines. *Mon. Not. R. Astron. Soc.* **2001**, *323*, 343–361. https://doi.org/10.1046/j.1365-8711.2001.04180.x.
120. Ponciano-Ojeda, F.; Hernández-Gómez, S.; López-Hernández, O.; Mojica-Casique, C.; Colín-Rodríguez, R.; Ramírez-Martínez, F.; Flores-Mijangos, J.; Sahagún, D.; Jáuregui, R.; Jiménez-Mier, J. Observation of the 5p3/2→6p3/2 electric-dipole-forbidden transition in atomic rubidium using optical-optical double-resonance spectroscopy. *Phys. Rev. A* **2015**, *92*, 042511.
121. Ponciano-Ojeda, F.; Hernández-Gómez, S.; López-Hernández, O.; Mojica-Casique, C.; Colín-Rodríguez, R.; Ramírez-Martínez, F.; Flores-Mijangos, J.; Sahagún, D.; Jáuregui, R.; Jiménez-Mier, J. Laser spectroscopy of the 5P3/2→6Pj (j = 1/2 and 3/2) electric dipole forbidden transitions in atomic rubidium *AIP Conf. Proc.* **2018**, *1950*, 0300011.
122. Ponciano-Ojeda, F.; Hernández-Gómez, S.; López-Hernández, O.; Mojica-Casique, C.; Colín-Rodríguez, R.; Ramírez-Martínez, F.; Flores-Mijangos, J.; Sahagún, D.; Jáuregui, R.; Jiménez-Mier, J. One step beyond the electric dipole approximation: An experiment to observe the 5p→6p forbidden transition in atomic rubidium *Am. J. Phys.* **2018**, *86*, 7.
123. Bhattacharya, M.; Haimberger, C.; Bigelow, N.P. Forbidden Transitions in a Magneto-Optical Trap. *Phys. Rev. Letts.* **2003**, *91*, 213004. https://doi.org/10.1103/PhysRevLett.91.213004.
124. Preston, D.W. Doppler-free saturated absorption: Laser spectroscopy. *Am. J. Phys.* **1996**, *64*, 1432. https://doi.org/10.1119/1.18457.

125. Grumer, J.; Zhao, R.; Brage, T.; Li, W.; Huldt, S.; Hutton, R.; Zou, Y. Coronal lines and the importance of deep-core-valence correlation in Ag-like ions. *Phys. Rev. A* **2014**, *89*, 062511. https://doi.org/10.1103/PhysRevA.89.062511.
126. Ding, X.B.; Koike, F.; Murakami, I. M1 transition energies and probabilities between the multiplets of the ground states of Ag-like ions with $Z = 47 - 92$. *J. Phys. B* **2012**, *45*, 035003. https://doi.org/10.1088/0953-4075/45/3/035003.
127. Basu, J.; Ray, D. Suppression of fine-structure splitting and oscillator strength of sodium D-line in a Debye plasma. *Phys. Plasmas* **2014**, *21*, 013301. https://doi.org/10.1063/1.4861880.
128. Xie, L.Y.; Wang, J.G.; Janev, R.K. Relativistic effects in the photoionization of hydrozen-like ions with screened coulomb interaction. *Phys. Plasmas* **2014**, *21*, 063304. https://doi.org/10.1063/1.4882244.
129. Sahoo, S.; Ho, Y.K. On the appearance of a Cooper Minimum in the Photoionization Cross Section of the Plasma-Embedded Li Atom. *Res. Lett. Phys.* **2009**, *2009*, 832413. https://doi.org/10.1155/2009/832413.
130. Buchet-Poulizac, M.C.; Buchet, J.P.; Ceyzeriat, P. Spectroscopic et durees de vie dand Ar VI-VII. *Nucl. Instrum. Methods* **1982**, *202*, 13–18. https://doi.org/10.1016/0167-5087(82)90369-6.
131. Johnson, W.R.; Liu, Z.W.; Sapirstein, J. Transition rates for lithium-like ions, sodium-like ions, and neutral alkali-metal atoms. *At. Data Nucl. Data Tables* **1996**, *64*, 279–300. https://doi.org/10.1006/adnd.1996.0024.
132. Knystautas, E.J.; Drouin, R.; Druetta, M. Nouvelles identification et mesures de durees de vie dans l'argon hautement ionise. *J. Phys. Colloques* **1979**, *40*, C1-186–C1-189. https://doi.org/10.1051/jphyscol:1979137.
133. Crossley, R.J.S.; Dalgarno, A. An expansion method for calculating atomic properties, V. Transition probabilities of M shell electrons. *Proc. R. Soc. A* **1965**, *286*, 510–518. https://doi.org/10.1098/rspa.1965.0160.
134. Livingston, A.E.; Irwin, D.J.G.; Pinnington, E.H. Lifetime measurement in Ar II-Ar VIII. *J. Opt. Soc. Am.* **1972**, *62*, 1303–1308. https://doi.org/10.1364/JOSA.62.001303.
135. Cheng, K.-T.; Kim, Y.-K. Excitation energy and oscillator strength in the silver isoelectronic sequence. *J. Opt. Soc. Am.* **1979**, *69*, 125. https://doi.org/10.1364/JOSA.69.000125.